

Pose Stabilization of a Bar Tethered to Two Aerial Vehicles

Pedro O. Pereira^a, Dimos V. Dimarogonas^a

^a*School of Electrical Engineering and Computer Science, KTH Royal Institute of Technology, SE-100 44, Stockholm, Sweden.*

Abstract

This work focuses on the modeling, control and analysis of a bar, tethered to two unmanned aerial vehicles, which is required to stabilize around a desired pose. We derive the equations of motion of the system, we close the loop by equipping each UAV with a PID control law, and finally we linearize the closed-loop vector field around some equilibrium points of interest. When requiring the bar to stay on the horizontal plane and under no normal stress, we verify that the bar's motion is decomposable into three decoupled motions, namely a longitudinal, a lateral and a vertical: for a symmetric system, each of those motions is further decomposed into two decoupled sub-motions, one linear and one angular; for an asymmetric system, we provide relations on the UAVs' gains that compensate for the system asymmetries and which decouple the linear sub-motions from the angular sub-motions. From this analysis, we provide conditions, based on the system's physical parameters, that describe *good* and *bad* types of asymmetries. Finally, when requiring the bar to pitch or to be under normal stress, we verify that there is a coupling between the longitudinal and the vertical motions, and that a positive normal stress (tension) has a positive effect on the stability, while a negative normal stress (compression) has a negative effect on the stability.

1. Introduction

Vertical take off and landing rotorcrafts, with hovering capabilities, provide a platform for transportation of cargos in dangerous and cluttered environments (*AEROWORKS*, 2018). In cluttered environments, transportation with a single UAV may be the only feasible option, while transportation with multiple UAVs is primarily necessary when the cargo exceeds the individual UAVs' payload capacity. However, transportation with multiple UAVs is inevitable if one wishes to control the pose of the cargo: in particular, controlling the pose of a bar requires a minimum of two UAVs, while controlling the pose of a generic rigid body requires a minimum of three UAVs (Jiang and Kumar, 2013).

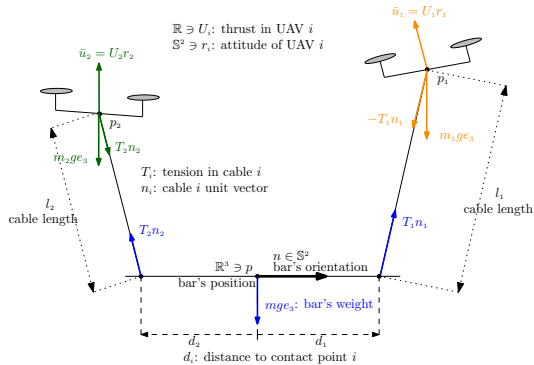
Using tethers in conjunction with UAVs can serve different and distinct purposes. Tethers/cables may be used to supply power or fuel to the UAV and thus to extend its flight time, or they may be used to provide an uninterrupted data transmission link (Nicotra et al., 2017; Schmidt and Swik, 1974; Tognon et al., 2016). However, in this paper, the purpose of the cables is to physically couple one or more UAVs to a cargo: when the cables are slack, the cargo is free of actuation; on the contrary, when they are taut, the cables provide an actuation medium for stabilizing the pose of the cargo. In this work, we assume that the cables are always taut, and thus that they behave as massless rigid links. A hybrid model, as in (Cruz et al., 2015; Marconi et al., 2011; Pounds and Dollar, 2014), can provide a more complete description of the dynamics of

tethered transportation by accounting for the hybrid behaviour of the cables. However, the focus of this paper is on the control design and analysis of the local closed-loop behavior, rendering a complete hybrid model of the system redundant.

Manipulator-endowed transportation (Korpela et al., 2013; Nguyen et al., 2015; Suarez et al., 2016) provides an alternative to tethered transportation. However, tethered transportation is mechanically simple and inexpensive, while robotic manipulators are heavy and therefore diminish the useful payload capacity a UAV can carry. Several control strategies for slung-load transportation, i.e., tethered transportation of a point-mass cargo by a single UAV, are found in the literature: the load swing can be dampened by appropriately planning trajectories, or by using vision and force measurements (Bisgaard et al., 2010; Lee and Kim, 2017; Palunko et al., 2012; Tang and Kumar, 2015; Tognon and Franchi, 2017); compensating for unknown model parameters can also be accomplished (Dai et al., 2014; Goodarzi and Lee, 2015); and, when the point-mass cargo exceeds the allowed UAV's payload, cooperative tethered transportation becomes imperative (Kondak et al., 2009; Lee et al., 2013; Pereira and Dimarogonas, 2017b).

This paper, on the other hand, focuses on transportation of a non-point-mass cargo. Control laws with an extended domain of operation and an extended domain of attraction are found in the literature (Lee, 2014, 2015; Pereira and Dimarogonas, 2017c), which can deal with asymmetries of the system but which lack experimental validation. On the other hand, cooperative transportation of rigid body cargos using simpler control laws has been tested and validated under various symmetry conditions (where UAVs are identical, cables are of the same length,

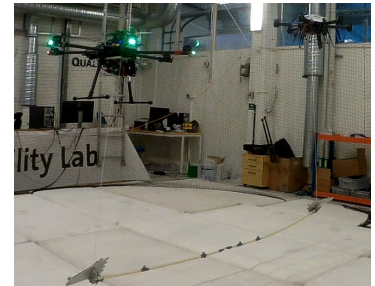
^{*}This work was supported by the EU H2020 Research and Innovation Programme under GA No.644128 (AEROWORKS), the Swedish Research Council (VR), the Swedish Foundation for Strategic Research (SSF) and the KAW Foundation.



(a) Modeling of the system (given the bar's orientation, $d_1 > 0$ and $d_2 < 0$).



(b) Symmetric system (Pereira and Dimarogonas, 2017a).



(c) Non-symmetric system (Pereira et al., 2018).

Figure 1: Tethered transportation of a rod-like object by two aerial vehicles (in a symmetric system, the UAVs are identical, the cables are of the same length, and the contact points are equally distanced away from the bar's center-of-mass).

and contact points are symmetrically distributed on the cargo) (Gassner et al., 2017; Jiang and Kumar, 2013; Kim et al., 2014; Lee et al., 2017; Michael et al., 2011). We emphasize that aerial cooperative tethered transportation comes with multiple degrees of freedom, which can be exploited to, for example, minimize the internal forces applied on the cargo (Masone et al., 2016; Mohammadi et al., 2016). In this manuscript, we focus on stabilization of a rod-like object tethered to two UAVs, as pictured in Fig. 1.

This problem has also been considered in (Gassner et al., 2017; Pereira and Dimarogonas, 2017a; Pereira et al., 2018; Tagliabue et al., 2017). In (Tagliabue et al., 2017), a master-slave approach for the two UAVs is adopted, where the UAV slave estimates the cable force exerted on itself. In (Gassner et al., 2017), vision is used to autonomously estimate the bar's pose. In (Pereira and Dimarogonas, 2017a; Pereira et al., 2018), relations on the UAVs' PID gains are provided for which stability – regarding the bar's pose stabilization – is guaranteed. We note that (Gassner et al., 2017; Pereira and Dimarogonas, 2017a; Pereira et al., 2018; Tagliabue et al., 2017) take the system to be symmetric and/or stabilize the bar on the horizontal plane and under no normal stress; whereas, in this paper, we relax both of these conditions. We perform an analysis similar to that in (Orsag et al., 2013; Pereira and Dimarogonas, 2017d; Pounds and Dollar, 2014), where we linearize the system, and derive conditions on the gains that guarantee exponential stability regarding the stabilization of the bar's pose. We note that the state-space of the system is a manifold, and for that reason we provide an analysis tool that allows us to linearize the vector field around a point in the state-space without having to provide a parameterization of the manifold.

The results of this paper are partially based on (Pereira and Dimarogonas, 2017a; Pereira et al., 2018), with the first focusing on the symmetric case, and the second focusing on the asymmetric case. This paper's main contributions, which we list next, are also the distinguishing factors with respect to the latter two works. (i) We derive the open-loop vector field, which is invariant to translations and rotations around the vertical direction, and we

describe and parametrize the open-loop equilibrium points and equilibrium inputs, from which we derive the necessity of integral action terms in the vertical direction of each UAV's control law – Section 3. (ii) We construct a PID-like control law, under which the closed-loop equilibria are entirely parameterizable with just two parameters, namely the desired pitch angle of the bar (θ_*), and the desired normal stress to be exerted on the bar (F_*) – Section 4. (iii) When $(\theta_*, F_*) = (0, 0)$, we show that the system's motion can be broken down into three decoupled motions (vertical, longitudinal and lateral), with each motion being composed of two sub-motions (one linear and one angular) – Sections 6.3 and 6.4. When $\theta_* \neq 0$ or $F_* \neq 0$, we show that the longitudinal and the vertical motions are no longer decoupled; we also find out that a bar under tension, as opposed to a bar under compression, is beneficial when it comes to stability – Sections 6.5 and 6.6. For the latter case, such an analysis is unique and novel among the literature on aerial transportation. For all the different cases, we provide conditions on the control law PID gains that guarantee that each and every motion/sub-motion is asymptotically stable, and therefore that the equilibrium of the non-linear system is (locally) exponentially stable. We also provide conditions, based on the system's physical parameters, that describe *good* and *bad* types of asymmetries: e.g., it is better for the heavier vehicle to be attached to the shorter cable, in the sense that stability is guaranteed by a smaller proportional gain. All the derivations described in the paper may also be verified in the Mathematica notebook files found in (Pereira and Dimarogonas, 2018).

2. Notation

The map $\mathcal{S} : \mathbb{R}^3 \rightarrow \mathbb{R}^{3 \times 3}$ yields a skew-symmetric matrix and it satisfies $\mathcal{S}(a)b = a \times b$, for any $a, b \in \mathbb{R}^3$. $S^2 := \{x \in \mathbb{R}^3 : x^T x = 1\}$ denotes the set of unit vectors in \mathbb{R}^3 . We denote $A_1 \oplus \dots \oplus A_n$ as the block diagonal matrix with block diagonal entries A_1 to A_n (square matrices). $df : \mathbb{R}^n \ni a \mapsto df(a) \in \mathbb{R}^{m \times n}$ denotes the derivative of a function $f : \mathbb{R}^n \rightarrow \mathbb{R}^m$. We denote by $e_1, \dots, e_n \in \mathbb{R}^n$ the canonical basis vectors in \mathbb{R}^n .

3. Problem Description

Consider the system illustrated in Fig. 1a, with two VTOL aerial vehicles, a one dimensional bar and two cables connecting the aerial vehicles to distinct contact points on the bar. Fig. 1a provides a two-dimensional picture of the real system, as shown in Figs. 1b and 1c, but the modeling we describe next is three dimensional. Hereafter, and for brevity, we refer to this system as UAVs-bar system. We denote by $p_1, p_2, p \in \mathbb{R}^3$ and by $v_1, v_2, v \in \mathbb{R}^3$ the UAVs' and the bar's center-of-mass positions and velocities; by $n, \omega \in \mathbb{R}^3$ the bar's angular position (orientation) and angular velocity; and by $r_1, r_2 \in \mathbb{S}^2$ the UAVs' thrust body directions. As for physical constants, we denote by $m_1, m_2, m > 0$ the UAVs' and bar's masses; by $J > 0$ the bar's moment of inertia (w.r.t. the bar's center-of-mass); by $l_1, l_2 > 0$ the cables' lengths; and, finally, by $d_1, d_2 \in \mathbb{R}$ the distance to the contact points on the bar at which the cables are attached (d_i is positive if it is along $+n \in \mathbb{S}^2$, and negative if it is along $-n \in \mathbb{S}^2$). Finally, we denote by $u_1, u_2 \in \mathbb{R}^3$ the input forces on the UAVs-bar system: for $j \in \{1, 2\}$, $\bar{u}_j := U_j r_j := u_j^T r_j r_j$ is the UAV's j input force, where the throttle U_j is taken as the inner product between the input u_j and the UAV's thrust direction r_j (one may think of u_j as the desired value for \bar{u}_j).

Consider then the position variables z_p , the velocity variables z_v , the thrust body directions r , the state z , and the input u defined as

$$z_p := (p, n, p_1, p_2) \in (\mathbb{R}^3)^4, z_v := (v, \omega, v_1, v_2) \in (\mathbb{R}^3)^4, \quad (1a)$$

$$r := (r_1, r_2) \in \mathbb{R}^{3+3}, z := (z_p, z_v, r) \in \mathbb{R}^{12+12+6}, \quad (1b)$$

$$u := (u_1, u_2) \in (\mathbb{R}^3)^2, \bar{u} := (u_1^T r_1 r_1, u_2^T r_2 r_2) \in (\mathbb{R}^3)^2. \quad (1c)$$

Given the position and the velocity variables in (1a), the system kinematics Z_p are given by

$$\dot{z}_p = Z_p(z) := \dot{z}_p = (I_3 \oplus \mathcal{S}(-n) \oplus I_3 \oplus I_3) z_v, \quad (2)$$

Consider then the map $f : \mathbb{R}^{30} \rightarrow \mathbb{R}^8$, whose domain where it vanishes encapsulates the constraints illustrated in Fig. 1a, defined as

$$f(z) := \begin{bmatrix} f_1(z_p) \\ f_2(z_p) \\ f_3(z_p, z_v) \\ f_4(z_p, z_v) \\ f_5(z_p) \\ f_6(z_p, z_v) \\ f_7(r_1) \\ f_8(r_2) \end{bmatrix} := \begin{bmatrix} l_1^{-2} \|p + d_1 n - p_1\|^2 - 1 \\ l_2^{-2} \|p + d_2 n - p_2\|^2 - 1 \\ df_1(z_p) Z_p(z) \\ df_2(z_p) Z_p(z) \\ n^T n - 1 \\ n^T \omega \\ r_1^T r_1 - 1 \\ r_2^T r_2 - 1 \end{bmatrix}. \quad (3)$$

Specifically, (the constraints' nomenclature we adopt here is the standard one; see, f.e., (Monforte, 2002)): f_1 and f_2 are geometric constraints imposed by the cables, which require that the distance between each contact point on the bar and the corresponding UAV is equal to the corresponding cable length. f_3 and f_4 are kinematic (holonomic) constraints which follow from differentiation of the previous two geometric constraints. f_5, f_7, f_8 are geometric constraints which imply that n, r_1, r_2 are unit vectors. And f_6 is a kinematic (nonholonomic) constraint, which implies that the bar's angular velocity ω is orthogonal to

the bar's angular position n , and thus that the bar does not rotate around itself.

The necessity for specifying the constraints is two-fold. First, when linearizing the closed-loop vector field around the desired equilibrium, the constraints imposed by f in (3) play a crucial role in examining whether the Jacobian matrix is Hurwitz or not (see Section 6). Secondly, it allows us to define the state-space and the tangent set to each point in the state-space, which, in turn, allows us to determine the tensions in each cable. Indeed, the constraints in (3) give rise to the state space and the tangent space given by

$$\mathbb{Z} := \{z \in \mathbb{R}^{30} : f(z) = 0_s\} \text{ and} \quad (4a)$$

$$T_z \mathbb{Z} := \{\dot{z} \in \mathbb{R}^{30} : df(z) \dot{z} = 0_s\}, \quad (4b)$$

where \mathbb{Z} is a manifold of dimension $22 = 30 - 8$ ($df(z) \in \mathbb{R}^{8 \times 30}$ is the derivative of f at z). For convenience, define $\mathbb{R}_0^6 := (\mathbb{R}^3 \setminus \{0_3\}) \times (\mathbb{R}^3 \setminus \{0_3\})$. Then, given an appropriate input $u : \mathbb{R}_{\geq 0} \rightarrow \mathbb{R}_0^6$, a system's trajectory $z : \mathbb{R}_{\geq 0} \rightarrow \mathbb{Z}$ evolves according to

$$\dot{z}(t) = Z(z(t), u(t)), z(0) \in \mathbb{Z}, \quad (5a)$$

where the vector field $Z : \mathbb{Z} \times \mathbb{R}_0^6 \ni (z, u) \mapsto Z(z, u) \in \mathbb{R}^{30}$ is given by

$$\dot{z} = Z(z, u) := \quad (5b)$$

$$\begin{bmatrix} \dot{z}_p \\ \dot{z}_v \\ \dot{r}_1 \\ \dot{r}_2 \end{bmatrix} := \begin{bmatrix} Z_p(z) \\ Z_v(z, \bar{u}) \Big|_{\bar{u} \text{ in (1c)}} \\ \mathcal{S} \left(k_{r,1} \mathcal{S}(r_1) \frac{u_1}{\|u_1\|} \right) r_1 \\ \mathcal{S} \left(k_{r,2} \mathcal{S}(r_2) \frac{u_2}{\|u_2\|} \right) r_2 \end{bmatrix} = \begin{bmatrix} \text{kinematics} \\ \text{dynamics} \\ \text{kinematics of } r_1 \\ \text{kinematics of } r_2 \end{bmatrix},$$

with the kinematics Z_p defined in (2), with the kinematics of the thrust body directions describing the attitude dynamics of each vehicle (and where $k_{r,i}$ is the positive attitude gain of vehicle i), and with the dynamics Z_v corresponding to the linear and the angular accelerations. The forces and their application points are depicted in Fig. 1a, which allows us to write down the dynamics Z_v of the system. For that purpose, and for convenience, consider the shorthand notations

$$n_i \equiv \frac{p_i - (p + d_i n)}{l_i} \in \mathbb{S}^2, \mathcal{T}_i \equiv T_i(z, \bar{u}) n_i \in \mathbb{R}^3, \quad (6)$$

where n_i is the unit vector associated to the cable i , and $T_i(z, \bar{u})$ is the tension on cable i (which depends on the state z and the input \bar{u}). Given the velocity variables, as introduced in (1a), the dynamics are then given by (below, g stands for the acceleration due to gravity)

$$\dot{z}_v = Z_v(z, \bar{u}) := \quad (7)$$

$$\begin{bmatrix} \dot{v} \\ \dot{\omega} \\ \dot{v}_1 \\ \dot{v}_2 \end{bmatrix} = \begin{bmatrix} -g e_3 \\ 0_3 \\ \frac{\bar{u}_1}{m_1} - g e_3 \\ \frac{\bar{u}_2}{m_2} - g e_3 \end{bmatrix} + \begin{bmatrix} \frac{n_1}{d_1 \mathcal{S}(n) n_1} & \frac{n_2}{d_2 \mathcal{S}(n) n_2} \\ \frac{J}{m_1} & \frac{J}{m_2} \\ 0_3 & -\frac{n_2}{m_2} \end{bmatrix} \begin{bmatrix} T_1(z, \bar{u}) \\ T_2(z, \bar{u}) \end{bmatrix},$$

where the tensions $T_1(z, \bar{u}), T_2(z, \bar{u})$ are found by solving the system of two equations $\frac{d}{dt}(f_3(z_p, z_v), f_4(z_p, z_v)) = (0, 0)$ (the result is found in (Pereira and Dimarogonas, 2018), omitted here for brevity, and without hindering comprehension). Note that one must verify that the vec-

tor field at a point lies in the respective tangent space, i.e., that $Z(z, u) \in T_z \mathbb{Z}$ for all $(z, u) \in \mathbb{Z} \times \mathbb{R}_0^6$, in order to guarantee that the state space \mathbb{Z} is indeed invariant. The latter check is easily performed: take for example the fifth constraint, which is indeed satisfied since $\frac{d}{dt} f_5(z_p, z_v) = \frac{d}{dt} n^T \omega = \dot{n}^T \omega + n^T \dot{\omega} = 0$.

3.1. Equilibria and Control Objective

In the previous section, we specified the vector field that describes the motion of our system, i.e., $\dot{z} = Z(z, u)$. In this section, we specify the open-loop equilibria: that is, given an input $u \in \mathbb{R}_0^6$, we determine the states $z \in \mathbb{Z}$ for which $Z(z, u) = 0_{30}$, leading to the set of equilibria $E_u := \{z \in \mathbb{Z} : Z(z, u) = 0_{30}\}$. The open-loop equilibria we describe next are illustrated in Fig. 2. As we verify next, in open-loop, there exists a continuum of equilibrium points, and therefore no such point is asymptotically stable. This provides the motivation for closing the loop, under an appropriate control law, which we specify in Section 4.

Let us then compute the equilibria, i.e., the states z for which $Z(z, u) = 0_{30}$. It follows from the kinematic of r_i in (5b), that $\dot{r}_i = 0_3 \Leftrightarrow \tilde{u}_i = u_i \Leftrightarrow r_i = \pm \frac{u_i}{\|u_i\|}$ (hereafter, we only consider $r_i = +\frac{u_i}{\|u_i\|}$, as all other possibilities lead to unstable equilibria). It follows from the first six equations in (7) that (recall (6) and recall also that the cables are connected to distinct contact points, i.e., that $d_1 \neq d_2$)

$$\begin{bmatrix} \dot{v} \\ \dot{\omega} \end{bmatrix} = \begin{bmatrix} 0_3 \\ 0_3 \end{bmatrix} \Leftrightarrow \begin{bmatrix} \mathcal{T}_1 \\ \mathcal{T}_2 \end{bmatrix} = \begin{bmatrix} \frac{d_2}{d_2-d_1} m g e_3 + F n \\ \frac{d_1}{d_1-d_2} m g e_3 - F n \end{bmatrix}, \quad (8a)$$

for any $F \in \mathbb{R}$, whose meaning will become clear next. It follows from the final six equations in (7) that

$$\begin{bmatrix} \dot{v}_1 \\ \dot{v}_2 \end{bmatrix} = \begin{bmatrix} 0_3 \\ 0_3 \end{bmatrix} \stackrel{(8a)}{\Leftrightarrow} \begin{bmatrix} u_1 \\ u_2 \end{bmatrix} = \begin{bmatrix} m_1 g e_3 + \frac{d_2}{d_2-d_1} m g e_3 + F n \\ m_2 g e_3 + \frac{d_1}{d_1-d_2} m g e_3 - F n \end{bmatrix} \quad (8b)$$

$$\Leftrightarrow \begin{bmatrix} (\delta_1 :=) u_1 + u_2 - (m_1 + m_2 + m) g e_3 \\ (\delta_2 :=) \frac{d_1(u_1 - m_1 g e_3) + d_2(u_2 - m_2 g e_3)}{d_1 - d_2} \end{bmatrix} = \begin{bmatrix} 0_3 \\ F n \end{bmatrix}. \quad (8c)$$

That is, (8b)–(8c) describe the conditions an input must satisfy in order to sustain an equilibrium. (i) Each UAV needs to cancel its own weight (term $m_i g e_3$ in (8b)). (ii) Each UAV needs to cancel some part of the bar's weight (term $\frac{d_i}{d_j - d_i} m g e_3$ in (8b)), and where the fraction of weight depends on the contact points on the bar. In particular, if $d_1 = -d_2$, then each UAV carries half of the bar's weight; on the other hand, if $|d_i| \gg |d_j|$ then UAV j carries most of the bar's weight. (iii) One UAV applies some force $F \in \mathbb{R}$ along the bar's angular position n , while the other applies an opposite force. For simplicity, let $d_1 > 0$ and $d_2 < 0$: if the force $F > 0$, then the bar is under tension and the UAVs are further away from each other; if the force $F < 0$, then the bar is under compression and the UAVs are closer to each other; and finally, if $F = 0$, the bar is under no normal force/stress – these cases are illustrated in Fig. 2.

Remark 1. Let $F = 0$ in (8a). If d_1, d_2 have opposite signs, then both cables are under tension. If d_1, d_2 have the same sign, then the cable with the smallest $|d_i|$ is under

tension, and the one with the largest is under compression, which is not possible for a cable. For that reason, hereafter, we assume that d_1 and d_2 have opposite signs.

Proposition 2. Let $u \in \mathbb{R}_0^6 \Leftrightarrow (u_1, u_2) \in (\mathbb{R}^3 \setminus \{0_3\}) \times (\mathbb{R}^3 \setminus \{0_3\})$ be some chosen input, such that $e_3^T u_1 > m_1 g$ and $e_3^T u_2 > m_2 g$. Denote $E_u := \{z \in \mathbb{Z} : z_v = 0_{12} \text{ and } (r_1, r_2) = (u_1/\|u_1\|, u_2/\|u_2\|) \text{ and } z_p = (p, n, p + d_1 n + l_1 n_1, p + d_2 n + l_2 n_2) \text{ for some } (p, n) \in \mathbb{R}^3 \times \mathbb{S}^2 \text{ and some } (n_1, n_2) \in \mathbb{S}^2 \times \mathbb{S}^2\}$ as the equilibria set for the input u . Consider then δ_1, δ_2 as defined in (8c). The following cases follow: (i) If $\delta_1 \neq 0_3$, then $E_u = \emptyset$. (ii) If $\delta_1 = 0_3$ and $\delta_2 = 0_3$, then E_u is that above for any $(p, n) \in \mathbb{R}^3 \times \mathbb{S}^2$ and with $n_i = \frac{u_i - m_i g e_3}{\|u_i - m_i g e_3\|} \in \mathbb{S}^2$. (iii) If $\delta_1 = 0_3$ and $\delta_2 \neq 0_3$, then E_u is that above for any $(p, n) \in \mathbb{R}^3 \times \{\pm \delta_2 / \|\delta_2\|\}$ and with $n_i = \frac{u_i - m_i g e_3}{\|u_i - m_i g e_3\|} \in \mathbb{S}^2$.

A proof is found in (Pereira and Dimarogonas, 2018). Proposition 2 provides some insight into the problem. Firstly, there are two non-binding conditions (inequalities), namely $e_3^T u_1 > m_1 g$ and $e_3^T u_2 > m_2 g$ which guarantee that, at the equilibrium, both cables are pointing up ($e_3^T n_i = \frac{e_3^T u_i - m_i g}{\|u_i - m_i g e_3\|} > 0$). There are however three binding conditions (equalities), namely $\delta_1 = 0_3 \Leftrightarrow u_1 + u_2 = (m_1 + m_2 + m) g e_3$. It follows from the latter that $e_3^T \delta_1 = 0 \Leftrightarrow e_3^T (u_1 + u_2) = (m_1 + m_2 + m) g$, which states that the combined inputs need to compensate for the combined weight of the whole system. This binding condition on the inputs is hard to satisfy since one does not exactly know the weights of the UAVs and of the bar; in experiments, it is therefore important to include, on each UAV, an integrator in the vertical direction so that the latter binding condition can be satisfied. Two more binding conditions follow from $\delta_1 = 0_3$, namely $e_1^T \delta_1 = 0$ and $e_2^T \delta_1 = 0$: when $F = 0$ (no normal force applied on the bar), these conditions are met when $e_1^T u_i = e_2^T u_i = 0$ (no horizontal input from both UAVs), where the latter conditions are easy to satisfy (and the main reason for not including integrators in the horizontal components).

Proposition 2 also tells us that no equilibrium is asymptotically stable in open-loop, since E_u in (ii) and (iii) corresponds to a continuum of equilibria. However, when the condition $\delta_2 \neq 0_3$ is satisfied, the equilibrium angular position of the bar (i.e. n) is uniquely determined up to a sign: intuition suggests that one equilibrium attitude might be asymptotically stable – the one where the bar is under tension; while the diametrically opposed attitude might be unstable – the one where the bar is under compression.

In the experiments, only the scenario $\delta_2 = 0_3 \Leftrightarrow F = 0$ has been tested, that is, the scenario where the bar is under no normal force at the equilibrium. For this scenario (see (8b)), it follows that $u_1 = m_1 g e_3 + \frac{d_2}{d_2 - d_1} m g e_3$ and that $u_2 = m_2 g e_3 + \frac{d_1}{d_1 - d_2} m g e_3$. That is, at the equilibrium, the UAVs do not need to provide any horizontal input, but only a vertical input. This is the main reason for, later on, including an integrator along the vertical direction, but not along the horizontal directions.

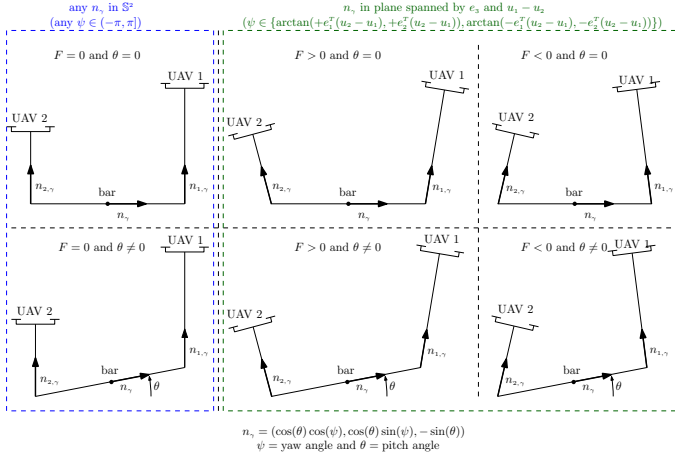


Figure 2: Different equilibria possibilities, for different values of the pitch angle of the bar – $\theta \in (-\frac{\pi}{2}, \frac{\pi}{2})$ – and different values of the normal force/stress exerted on the bar – $F \in \mathbb{R}$. When $F > 0$, the bar is under tension; when $F < 0$, the bar is under compression; and, when $F = 0$, the bar is under no normal force.

Let us now parametrize the equilibria with

$$\gamma \in \Gamma : \Leftrightarrow (p_\gamma, n_\gamma, F_\gamma) \in \mathbb{R}^3 \times \mathbb{S}^2 \times \mathbb{R}, \quad (9)$$

where $(p_\gamma, n_\gamma) \in \mathbb{R}^3 \times \mathbb{S}^2$ is the desired pose (desired linear and angular positions) for the bar; and $F_\gamma \in \mathbb{R}$ is the desired normal force to be exerted on the bar. The variable γ in (9) is a six-dimensional variable that allows us to parametrize the equilibrium input and the corresponding equilibria. That is, any point in the set $E := \{(z, u) \in \mathbb{Z} \times \mathbb{R}_0^6 : Z(z, u) = 0_{2,4}\}$ can be parametrized by some $\gamma \in \Gamma$, i.e., $E = \{(z_\gamma, u_\gamma) \in \mathbb{Z} \times \mathbb{R}_0^6 : \gamma \in \Gamma\}$, with (z_γ, u_γ) as described next. The equilibrium input u_γ is parametrized by n_γ and F_γ as

$$u_\gamma := \begin{bmatrix} u_{1,\gamma} \\ u_{2,\gamma} \end{bmatrix} := \begin{bmatrix} \left(m_1 + \frac{d_2}{d_2 - d_1} m\right) g e_3 + F_\gamma n_\gamma \\ \left(m_2 + \frac{d_1}{d_1 - d_2} m\right) g e_3 - F_\gamma n_\gamma \end{bmatrix}, \quad (11)$$

while the equilibrium state is parametrized as

$$z_\gamma := (z_{p,\gamma}, z_{v,\gamma}, r_{1,\gamma}, r_{2,\gamma}) := \left(z_{p,\gamma}, 0_{1,2}, \frac{u_{1,\gamma}}{\|u_{1,\gamma}\|}, \frac{u_{2,\gamma}}{\|u_{2,\gamma}\|} \right) \quad (12)$$

$$z_{p,\gamma} := (p_\gamma, n_\gamma, p_{1,\gamma}, p_{2,\gamma}) \text{ with}$$

$$p_{j,\gamma} := p_\gamma + d_j n_\gamma + l_j \frac{d_j m g e_3 \pm (d_j - d_i) F_\gamma n_\gamma}{\|d_j m g e_3 \pm (d_j - d_i) F_\gamma n_\gamma\|},$$

Figure 2 illustrates the different possible equilibrium configurations.

At this point, we can state our control objective, which consists in designing a control law that guarantees pose stabilization of the bar around a desired linear position p_γ and around a desired angular position n_γ , and such that the bar is under a desired normal force F_γ .

Problem 1. Let $\gamma \in \Gamma$, as in (9), be some chosen desired configuration. Consider then the vector field Z in (5b), the equilibrium state z_γ in (12), and the equilibrium input u_γ in (11). Design a control law $u_\gamma^{cl} : \mathbb{Z} \rightarrow \mathbb{R}^6$ satisfying $u_\gamma^{cl}(z_\gamma) = u_\gamma$ and such that z_γ is a (locally) exponentially stable equilibrium point of the closed-loop vector field $\tilde{Z} \ni z \mapsto Z(z, u_\gamma^{cl}(z)) \in T_z \mathbb{Z}$.

Hereafter, given some $\theta_* \in (-\frac{\pi}{2}, +\frac{\pi}{2})$ and $F_* \in \mathbb{R}$, instead of a generic γ in (9), we only consider

$$\gamma^* := (p_{\gamma^*}, n_{\gamma^*}, F_{\gamma^*}) := (0_3, (\cos(\theta_*), 0, \sin(\theta_*)), F_*). \quad (13)$$

In brief, and loosely speaking, this simplification can be made because the open-loop vector field Z is invariant to translations and to rotations around the vertical direction, and because the control laws we provide next are also invariant to translations and to rotations: the latter imply that the closed-loop vector field is invariant to translations and to rotations, which means we may consider only the case where we wish to stabilize the bar's linear position around the origin and to stabilize the bar's angular position aligned with the first inertial axis and titled by an angle θ_* . A formal and detailed description of the latter points is provided in (Pereira and Dimarogonas, 2018).

4. Control Law

Recall the problem statement in Problem 1, where a desired pose and normal force are chosen, encapsulated in $\gamma = (p_\gamma, n_\gamma, F_\gamma)$. Whatever control law we design, at the equilibrium it must match u_γ in (11): suppose, for simplicity, that we wish the bar to be under no normal force, that is, $F_\gamma = 0$; then, it follows from (11) that $u_{1,\gamma} = \left(m_1 g + \frac{d_2}{d_2 - d_1} m g\right) e_3$, that is, UAV 1 needs to have an exact knowledge of its weight, of the bar's weight, and of the contact points on the bar (an interchangeable conclusion may be drawn for UAV 2). Note, however, that only the third (vertical) component of $u_{1,\gamma}$ is model dependent, while the first and second (horizontal) components are zero and, therefore, model independent. This is the motivation for including an integral action in the vertical component of the control laws of each UAV (and to suppress such integral action in the horizontal components).

For that purpose, and with the latter in mind, define now the extended state, constraints, and state space

$$\tilde{\mathbb{Z}} \in \mathbb{R}^{3,2} : \Leftrightarrow (z, \xi_{1,z}, \xi_{2,z}) \in \mathbb{R}^{3,0} \times \mathbb{R} \times \mathbb{R}, \quad (14a)$$

$$\tilde{f}(\tilde{z}) := f(z)|_{f \text{ in (3)}}, \quad (14b)$$

$$\tilde{\mathbb{Z}} := \{\tilde{z} \in \mathbb{R}^{3,2} : \tilde{f}(\tilde{z}) = 0_s\} = \mathbb{Z} \times \mathbb{R} \times \mathbb{R}, \quad (14c)$$

where $\xi_{1,z}, \xi_{2,z}$ are the integral action terms for UAVs 1 and 2. Then, given an appropriate input $u : \mathbb{R}_{\geq 0} \rightarrow \mathbb{R}_0^6$, a system's trajectory $\tilde{z} : \mathbb{R}_{\geq 0} \rightarrow \tilde{\mathbb{Z}}$ evolves according to

$$\dot{\tilde{z}}(t) = \tilde{Z}_\gamma(\tilde{z}(t), u(t)), \tilde{z}(0) \in \tilde{\mathbb{Z}}, \quad (15a)$$

where the vector field $\tilde{Z}_\gamma : \tilde{\mathbb{Z}} \times \mathbb{R}_0^6 \ni (\tilde{z}, u) \mapsto \tilde{Z}_\gamma(\tilde{z}, u) \in T_{\tilde{z}} \tilde{\mathbb{Z}}$ is given by (the vector field depends on γ , and thus the reason for indexing γ in \tilde{Z}_γ)

$$\dot{\tilde{z}} = \tilde{Z}_\gamma(\tilde{z}, u) : \Leftrightarrow \begin{bmatrix} \dot{z} \\ \dot{\xi}_{1,z} \\ \dot{\xi}_{2,z} \end{bmatrix} = \begin{bmatrix} Z(z, u) \\ e_3^T (p_1 - p_{1,\gamma}) \\ e_3^T (p_2 - p_{2,\gamma}) \end{bmatrix}, \quad (15b)$$

where Z is the vector field defined in (5b), and where $p_{j,\gamma}$ is defined in (12). The integral action equations in (15b) enforce that an equilibrium can only be reached if the UAVs are at the desired height, i.e., if $e_3^T (p_i - p_{i,\gamma}) = 0$.

For $j \in \{1, 2\}$, denote $\hat{u}_{j,\gamma}$ as the best estimate of $u_{j,\gamma}$ known by UAV j ($u_{j,\gamma}$ defined in (11)). Given a γ , consider then the control law u_γ^{pid} , combining a feed-forward (FF) term with a proportional-derivative (PD) term and with an integral (I) term, given by

$$\tilde{z} \mapsto u_\gamma^{pid}(\tilde{z}) := \underbrace{\begin{bmatrix} \hat{u}_{1,\gamma} \\ \hat{u}_{2,\gamma} \end{bmatrix}}_{\text{FF term}} + \underbrace{\begin{bmatrix} \tilde{u}_{1,\gamma}^{pd}(z) \\ \tilde{u}_{2,\gamma}^{pd}(z) \end{bmatrix}}_{\text{PD term}} + \underbrace{\begin{bmatrix} m_1 k_{i,z}^1 \xi_{1,z} e_3 \\ m_2 k_{i,z}^2 \xi_{2,z} e_3 \end{bmatrix}}_{\text{I term}}, \quad (16)$$

where $\xi_{j,z}$ is the integral action term for UAV j , and $k_{i,z}^j$ is the respective integral gain; and where $\tilde{u}_{j,\gamma}^{pd}$ is the PD control law given by (below, we only provide the control law for γ^* defined in (13); for a general γ , some rotations need to be introduced, and the control law in that general case is found in (Pereira and Dimarogonas, 2018))

$$\begin{aligned} \tilde{u}_{j,\gamma^*}^{pd}(z) := & -m_j (K_p^j(p_j - p_{j,\gamma^*}) + K_d^j v_j) \\ & - m_j d_j e_3^T (k_{p,\psi}^j \mathcal{S}(n_{\gamma^*}) n + k_{d,\psi}^j \omega) e_2, \end{aligned} \quad (17)$$

and where for $j \in \{1, 2\}$: (i) $p_{j,\gamma} \in \mathbb{R}^3$ is the UAV j desired equilibrium position given in (12); (ii) $K_p^j = k_{p,x}^j \oplus k_{p,y}^j \oplus k_{p,z}^j \in \mathbb{R}^{3 \times 3}$ and $K_d^j = k_{d,x}^j \oplus k_{d,y}^j \oplus k_{d,z}^j \in \mathbb{R}^{3 \times 3}$ are positive gains related to the position and velocity feedback of UAV j ; (iii) $k_{p,\psi}^j \in \mathbb{R}_{\geq 0}$ and $k_{d,\psi}^j \in \mathbb{R}_{\geq 0}$ are gains related to the angular position and angular velocity feedback.

Let us provide some insight into the control law in (17), and recall that we wish to steer the linear position of the bar p to p_γ and to steer the angular position of the bar n to n_γ . Finally, and for brevity, let us introduce the following nomenclature: e_1 corresponds to the longitudinal direction, or x -direction; e_2 corresponds to the lateral direction, or y -direction; and e_3 corresponds to the vertical direction, or z -direction. The control law in (17) may be decomposed in two identifiable parts. (i) Along each component – longitudinal, lateral and vertical – there are two terms, one proportional and one derivative, that act as a spring-damper that brings the UAV to its desired longitudinal/lateral/vertical position. (ii) In addition, along the lateral component, there are two more terms (one proportional and one derivative) that assist in bringing the bar to its desired angular position.

As required by Problem 1, the input at the equilibrium must match u_γ : since $\tilde{u}_\gamma^{pid}(z_\gamma) = 0_6$, it follows immediately that for

$$\tilde{z}_\gamma := \begin{bmatrix} z_\gamma \\ \xi_{1,z,\gamma} \\ \xi_{2,z,\gamma} \end{bmatrix} := \begin{bmatrix} z_\gamma \\ \frac{1}{m_1 k_{i,z}^1} e_3^T (u_{1,\gamma} - \hat{u}_{1,\gamma}) \\ \frac{1}{m_2 k_{i,z}^2} e_3^T (u_{2,\gamma} - \hat{u}_{2,\gamma}) \end{bmatrix}, \quad (18)$$

it holds that $u_\gamma^{pid}(\tilde{z}_\gamma) = u_\gamma$, and therefore \tilde{z}_γ is an equilibrium point of the closed-loop vector field

$$\tilde{Z} \ni \tilde{z} \mapsto \tilde{Z}_\gamma(\tilde{z}, u_\gamma^{pid}(\tilde{z})) \in T_{\tilde{z}} \tilde{Z}. \quad (19)$$

Note that it is the purpose of the integral action terms to make sure that the equality $u_\gamma^{pid}(\tilde{z}_\gamma) = u_\gamma$ is satisfied. Loosely speaking, the integral action terms $\xi_{1,z}, \xi_{2,z}$ evolve so as to compensate for the model mismatch; in particular, if all model parameters are exactly known by both UAVs, then $\xi_{1,z,\gamma} = \xi_{2,z,\gamma} = 0$.

The control law in (16) is unbounded (that is, $\|u_{j,\gamma}^{pid}(\tilde{z})\|$

is arbitrarily large when the UAV's linear position p_j is arbitrarily far away from its desired linear position $p_{j,\gamma}$): this motivates the introduction of saturation functions, which is done in (Pereira and Dimarogonas, 2018). However, in the next Sections we perform a linearization procedure, and one can easily show that the saturation functions do not play a role after the linearization, which is the reason why we omit them here for brevity.

5. Conditions for Local Stability

In Section 6, we linearize the closed-loop vector field around the equilibrium, and we verify that the Jacobian is similar to a block triangular matrix, whose block diagonal entries are in controllable form. This section provides tools for the analysis of the location of the eigenvalues of those matrices. Let $n \in \mathbb{N}$, and denote $C_n(a) := [e_2 \ \dots \ e_n \ -a]^T \in \mathbb{R}^{n \times n}$ as a matrix in controllable form, with $a \in \mathbb{R}$ and e_i as the i th canonical basis vector in \mathbb{R}^n . It follows from the Routh's criterion that

$$C_3((a_0, a_1, a_2)) \text{ Hurwitz} \Leftrightarrow a_0, a_1, a_2 > 0 \wedge a_0 < a_1 a_2, \quad (20)$$

which we make use of later on. In what follows, denote $q \in \mathbb{R}$, $f := (f_p, f_d) \in (\mathbb{R}_{\geq 0})^2$, $k := (k_p, k_d) \in (\mathbb{R}_{\geq 0})^2$, where, in later sections, q and f provide physical constants of interest, and k provides the controller gains (in particular a proportional and a derivative gain). There are matrices (in controllable form) that appear several times in Section 6, and therefore we introduce them here, namely

$$\Gamma_3(f, k) := C_3((f_d(k_p + f_p), f_d k_d + f_p, f_d)), \quad (21a)$$

$$\Gamma_5(q, f, k) := C_5(b_1 + b_2) \Big|_{\substack{b_1 \equiv f_d(f_p k_p, f_p k_d, k_p, k_d, 1) \\ b_2 \equiv f_p(1+q)(0, 0, f_d, 1, 0)}}, \quad (21b)$$

$$\tilde{\Gamma}_4(\tilde{q}, q, f_p, k) := C_4((f_p(k_p + f_p q \tilde{q}), f_p k_d, k_p + f_p(1+q), k_d)),$$

$$\Gamma_4(q, f_p, k) := \tilde{\Gamma}_4(0, q, f_p, k), \quad (21c)$$

and, it follows from the Routh's criterion that,

$$\Gamma_3(f, k) \text{ is Hurwitz} \Leftrightarrow f_d > k_p/k_d, \quad (22a)$$

$$\Gamma_5(q, f, k) \text{ is Hurwitz} \Leftrightarrow q > 0 \text{ and } f_d > k_p/k_d, \quad (22b)$$

$$\tilde{\Gamma}_4(\tilde{q}, q, f_p, k) \text{ is Hurwitz} \Leftrightarrow q(1 - \tilde{q}) > 0 \text{ and } k_p > -f_p q \tilde{q},$$

$$\Gamma_4(q, f_p, k) \text{ is Hurwitz} \Leftrightarrow q > 0. \quad (22c)$$

6. Stability Analysis of the Closed-Loop System

6.1. Linearization around a point in a manifold

Before linearizing the closed-loop vector field \tilde{Z}_γ^{cl} in (19) around the equilibrium \tilde{z}_γ in (18), let us provide a vector field that serves only the purpose of analysis. Consider then the constraints, the state space and the vector field

$$f : \mathbb{R}^n \ni y \mapsto f(y) \in \mathbb{R}^m, \quad (23a)$$

$$\mathbb{Y} := \{y \in \mathbb{R}^n : f(y) = 0_m\}, \quad (23b)$$

$$Y : \mathbb{Y} \ni y \mapsto Y(y) \in T_y \mathbb{Y}, \quad (23c)$$

where the vector field Y vanishes at $y^* \in \mathbb{Y}$, and $df(y^*) \in \mathbb{R}^{m \times n}$ is full rank. The following result follows.

Proposition 3. *Let Y be a vector field in \mathbb{Y} , as defined in (23), and with $y^* \in \mathbb{Y}$ as an equilibrium point (e.q.). Then, y^* is an exponentially stable e.q. of Y if and only if y^* is an exponentially stable e.q. of*

$$Y^*(y) := Y(y) - P_\perp^T (P_\perp P_\perp^T)^{-1} (df(y)Y(y) + \lambda f(y)), \quad (24)$$

where $P_\perp = df(y^*) \in \mathbb{R}^{m \times n}$, and where λ is some positive number. Moreover, given a change of basis $P := [P_1^T \ P_\perp^T]^T \in \mathbb{R}^{n \times n}$, with $P^{-1} \equiv [Q_1 \ Q_2]$, it follows that

$$PdY^*(y^*)P^{-1} = \begin{bmatrix} P_1 \Pi_{P_\perp} dY(y^*) \Pi_{P_\perp} Q_1 & \star_{(n-m) \times m} \\ 0_{m \times (n-m)} & -\lambda I_m \end{bmatrix}, \quad (25)$$

where $\Pi_{P_\perp} := I_n - P_\perp^T (P_\perp P_\perp^T)^{-1} P_\perp \in \mathbb{R}^{n \times n}$.

A proof of Proposition 3 is found in (Pereira and Dimarogonas, 2018), and its purpose is simple: in order to determine the stability properties of the equilibrium y^* , it suffices to study whether the upper-left matrix in (25) is Hurwitz. It is now obvious why we needed to provide the constraints' maps f and \tilde{f} defined in (3) and (14).

6.2. Linearization of the closed-loop vector field

Recall now the closed-loop vector field \tilde{Z}_γ^{cl} in (19) and the equilibrium point \tilde{z}_γ in (18). Hereafter, and for reasons already discussed, we consider only γ^* in (13). Given Proposition 3, we modify the vector field \tilde{Z}_γ^{cl} as in (24), and obtain the vector field $(\tilde{Z}_{\gamma^*}^{cl})^*$, which serves only the purpose of analysis. We then compute the Jacobian

$$A := d(\tilde{Z}_{\gamma^*}^{cl})^*(\tilde{z}_{\gamma^*}) \in \mathbb{R}^{32 \times 32} |_{(\tilde{Z}_{\gamma^*}^{cl})^*} \text{ as defined in (24)}, \quad (26)$$

which is sparse, but unstructured. Moreover, the Jacobian is neither a diagonal nor a triangular matrix, and thus determining whether it is Hurwitz is not straightforward. For that purpose, we provide a change of basis matrix $P := [P_1 \ \dots \ P_k \ P_\perp]^T$, for some $k \in \mathbb{N}$, such that PAP^{-1} is a block triangular matrix, i.e.,

$$PAP^{-1} = \begin{bmatrix} A_1 \oplus \dots \oplus A_k & \star \\ 0 & -\lambda I \end{bmatrix}. \quad (27)$$

That is, we provide a change of basis that breaks the motion of the system into k decoupled motions (note that $\lambda > 0$ in (27) is that chosen in (24)). Thus $\text{eig}(A) = \{-\lambda\} \cup \text{eig}(A_1) \cup \dots \cup \text{eig}(A_k)$, and, therefore, determining whether the Jacobian A in (26) is Hurwitz amounts to checking whether each of the blocks in (27) is Hurwitz.

In the next four subsections, we analyze four separate cases: in Section 6.3, we assume that the system is symmetric and that $(\theta_*, F_*) = (0, 0)$; in Section 6.4, we let the system be asymmetric, while still requiring that $(\theta_*, F_*) = (0, 0)$; in Section 6.5, we let $\theta_* \neq 0$ and $F_* = 0$; and, finally, in Section 6.6, we let $\theta_* = 0$ and $F_* \neq 0$ (for simplicity, in both Sections 6.5 and 6.6 we let the UAVs be fully actuated). Analyzing the most generic of cases (one where the system is asymmetric, the pitch is non-zero, and the normal force is also non-zero) may be done following a similar approach, but it is left for future research.

6.3. Symmetric UAVs-bar system

Let us discuss first the case where the UAVs-bar system is symmetric, i.e., when the cables have the same length;

when the contacts points on the bar are at the same distance away from the bar's center-of-mass (but in opposite directions); and, when the UAVs are identical, with the same weights and the same control law gains (and where we let $k_{p,\psi}^j = 0$ and $k_{d,\psi}^j = 0$ for $j \in \{1, 2\}$). These conditions are summarized in (42). This case provides us with intuition on how to decompose the Jacobian into three decoupled motions (vertical, longitudinal and lateral), and it is the basis for the generic case where the system does not satisfy the symmetry conditions in (42).

Consider then the Jacobian A in (26), and the change of basis matrix

$$P := [P_z \ P_\theta \ P_x \ P_\delta \ P_y \ P_\psi \ P_\perp]^T \in \mathbb{R}^{32 \times 32}, \quad (28)$$

with its entries listed in Table 1, and where $P_\perp := (d\tilde{f}(\tilde{z}_\gamma))^T \in \mathbb{R}^{32 \times 8}$ (\tilde{f} in (14b) – see Section 6.1). It can be calculated that $|P| = -\frac{d^3 g^{13} m^3 (m+2M)^4}{4J^3 L^{13} M^4}$, which is non-zero since $d \neq 0$. Given the state matrix A in (26) and the change of basis P in (28), it then follows that

$$PAP^{-1} = \begin{bmatrix} A_z \oplus A_\theta \oplus A_x \oplus A_\delta \oplus A_y \oplus A_\psi & \star \\ 0_{8 \times 24} & -\lambda I_{8 \times 8} \end{bmatrix}, \quad (29)$$

whose entries are listed in Table 1.

Remark 4. *Recall the state decomposition in (14a) (which builds upon (1b)), and that $\dot{\tilde{z}} = A\tilde{z}$, for the linearized motion around the equilibrium. Then (for brevity, denote $p = (x, y, z)$ and $n = (\cdot, \psi, \theta)$)*

$$\begin{bmatrix} P_x^T z \\ P_\delta^T z \\ P_y^T z \\ P_\psi^T z \end{bmatrix} = \begin{bmatrix} (x^{(0)}, x^{(1)}, x^{(2)}, x^{(3)}, x^{(4)}) \\ (\delta^{(0)}, \delta^{(1)}, \delta^{(2)}) |_{\delta=e_1^T(p_1-p_2)} \\ (y^{(0)}, y^{(1)}, y^{(2)}, y^{(3)}, y^{(4)}) \\ (\psi^{(0)}, \psi^{(1)}, \psi^{(2)}, \psi^{(3)}, \psi^{(4)}) \end{bmatrix},$$

and (the equalities below can only be verified under an appropriate coordinate transformation – see (Pereira and Dimarogonas, 2017a))

$$\begin{bmatrix} P_z^T z \\ P_\theta^T z \end{bmatrix} = \begin{bmatrix} (z^{(-1)}, z^{(0)}, z^{(1)}) \\ (\theta^{(-1)}, \theta^{(0)}, \theta^{(1)}) \end{bmatrix}.$$

That is, P_x is associated with the longitudinal (x) linear motion of the bar (fifth order system) and P_δ is associated with the longitudinal linear motion between the UAVs (third order system); P_y is associated with the lateral (y) linear motion of the bar (fifth order system) and P_ψ is associated with the lateral angular motion of the bar (fifth order system). And finally, P_z is associated with the vertical (z) linear motion of the bar (third order system) and P_θ is associated with the vertical angular motion of the bar (third order system): to be specific, the sum of the integral errors is associated with the vertical linear position of the bar, and the difference is associated with the vertical angular position of the bar.

6.3.1. Longitudinal motion

The matrices A_x and A_δ describe the linear and angular longitudinal motions and, it follows from (22b), that they are Hurwitz provided that

$$k_r > k_{p,x}/k_{d,x}. \quad (30)$$

i.e., provided that the attitude inner-loop gain is big enough. Since $P_x z = e_1^T p =: x$ and $P_\delta z = e_1^T (p_1 - p_2) =: \delta$, it follows from (29) that, for the linearized motion, the bar's x -position behaves as a fifth-order integrator and the longitudinal displacement between UAVs behaves as a third-order integrator, i.e.,

$$\begin{aligned} x^{(5)}(t) &= (A_x)_{5,5} x^{(4)}(t) + \dots + (A_x)_{5,1} x^{(0)}(t), \\ \delta^{(3)}(t) &= (A_\delta)_{3,3} \delta^{(2)}(t) + \dots + (A_\delta)_{3,1} \delta^{(0)}(t). \end{aligned}$$

6.3.2. Lateral motion

The matrices A_y and A_ψ describe the linear and angular lateral motions and, it follows from (22b), that they are Hurwitz provided that

$$k_r > k_{p,y}/k_{d,y}, \quad (31)$$

i.e., provided that the attitude inner-loop gain is big enough. Since $P_y z = e_2^T p =: y$ and $P_\psi z = e_2^T n =: \psi$, it follows from (29) that, for the linearized motion, the bar's lateral linear motion and the bar's lateral angular motion behave as fifth-order integrators, i.e.,

$$\begin{aligned} y^{(5)}(t) &= (A_y)_{5,5} y^{(4)}(t) + \dots + (A_y)_{5,1} y^{(0)}(t), \\ \psi^{(5)}(t) &= (A_\psi)_{5,5} \psi^{(4)}(t) + \dots + (A_\psi)_{5,1} \psi^{(0)}(t). \end{aligned}$$

6.3.3. Vertical motion

The matrices A_z and A_θ describe the linear and angular vertical motions and, it follows from (20), that they are both Hurwitz provided that

$$k_{i,z} < \min(\gamma_z, \gamma_\theta) k_{p,z} k_{d,z}. \quad (32)$$

i.e., provided that the integral gain is *small enough*. Note that, for a standard PID (i.e., $\dot{x} = C_3(-k_i, k_p, k_d)x$), it is required that $k_{i,z} < k_{p,z} k_{d,z}$, while the constraint above is more restrictive, since $\gamma_z < 1$ and $\gamma_\theta < 1$ (see Table 1). Moreover, notice that γ_θ vanishes when d vanishes (the distance of the contact points to the bar's center-of-mass): as such, it is advisable to have a *big* d (*big* compared to $\sqrt{\frac{J}{2M}}$), because γ_θ is closer to 1 (and thus the bound on the integral gain is less restrictive). This also agrees with intuition, which suggests that controlling the bar's attitude when the contact points are too close to the bar's center-of-mass is difficult. Under an appropriate coordinate change (Pereira and Dimarogonas, 2017a), it can be verified that the sum of the integral errors is related to the vertical linear position of the bar (i.e., if $z^{(-1)} \equiv \frac{d_2 \xi_{1,z} - d_1 \xi_{2,z}}{d_2 - d_1}$ then $z^{(1)} \equiv \frac{d^2}{dt^2} \frac{d_2 \xi_{1,z} - d_1 \xi_{2,z}}{d_2 - d_1} = v_z$), while the difference between the integral errors is related to the vertical angular position of the bar (i.e., if $\theta^{(-1)} \equiv \frac{\xi_{1,z} - \xi_{2,z}}{d_2 - d_1}$ then $\theta^{(1)} \equiv \frac{d^2}{dt^2} \frac{\xi_{1,z} - \xi_{2,z}}{d_2 - d_1} = \omega_y$). As such, for the linearized motion,

$$\begin{aligned} z^{(2)}(t) &= (A_z)_{3,3} z^{(1)}(t) + (A_z)_{3,2} z^{(0)}(t) + (A_z)_{3,1} z^{(-1)}(t), \\ \theta^{(2)}(t) &= (A_\theta)_{3,3} \theta^{(1)}(t) + (A_\theta)_{3,2} \theta^{(0)}(t) + (A_\theta)_{3,1} \theta^{(-1)}(t). \end{aligned}$$

At this point, we defer the presentation of our main result (Theorem 8) till the end on the next subsection, which considers the generic case where the system is asymmetric.

Remark 5. We emphasize that, for the linearized motion, and for $h \in \{x, y, z\}$, the proportional and derivative gains $k_{p,h}$ and $k_{d,h}$ have an effect on the h -motion only, which agrees with intuition. This is however not the case when the bar is required to be under normal stress ($F_* \neq 0$) nor when the bar is required to have a non-zero pitch ($\theta_* \neq 0$) – see Sections 6.5 and 6.6. Note also that the attitude gains of the vehicles do not play a role in the linearized vertical motion.

6.4. Asymmetric UAVs-bar system

Let us now consider the case where the system is not symmetric, i.e., a system which does not satisfy the conditions in (42) (we assume only that d_1, d_2 have opposite signs – see Remark 1). The idea will be to choose the UAVs' gains so as to compensate for the asymmetries, in such a way that, if the system degenerates into a symmetric one, then the results of the previous section are recovered.

Consider again the similarity matrix $P \in \mathbb{R}^{32 \times 32}$ as defined in (28) (which will be different than the P obtained in the previous section, which relied on the symmetry conditions), and whose determinant $|P|$ is non-zero when d_1 and d_2 have opposite signs.

Given the state matrix A in (26) and the similarity matrix P in (28), it then follows that

$$PAP^{-1} = \begin{bmatrix} A_{z,\theta} \oplus A_{x,\delta} \oplus A_{y,\psi} & \star \\ 0_{8 \times 24} & -\lambda I_{8 \times 8} \end{bmatrix} \in \mathbb{R}^{32 \times 32}. \quad (33)$$

Similarly to the symmetric system, described in the previous section, there are three decoupled motions, namely a vertical, a longitudinal and a lateral. However, for the symmetric system, each of those motions was in turn composed of two decoupled sub-motions, one linear and one angular; that is not the case for the asymmetric system. The main idea explored next is to choose the control gains such that the linear sub-motion of the vertical/longitudinal/lateral motion is decoupled from the angular sub-motion. The difference with the case where the system is symmetric lies in that the linear and angular sub-motions are not decoupled. This will produce a state matrix that is similar to a block triangular matrix, which we are still able to analyze.

6.4.1. Longitudinal motion

Recall Remark 4, and note that P_x and P_δ are associated to $A_{x,\delta} \in \mathbb{R}^{8 \times 8}$ in (33). As such, $A_{x,\delta}$ is associated with the longitudinal motion, namely the longitudinal linear motion of the bar, and the longitudinal angular motion (corresponding to the longitudinal relative motion between the two UAVs). In what follows denote $F_x \equiv F_x(k_{p,x}^1, k_{p,x}^2, k_{d,x}^1, k_{d,x}^2, k_r^1, k_r^2) \in \mathbb{R}^3$, where F_x is some function of the listed gains (found in the mathematica files in (Pereira and Dimarogonas, 2018)). Note then that $A_{x,\delta}$ has a specific structure, namely (below \star denotes a vector in \mathbb{R}^5)

$$A_{x,\delta} = \begin{bmatrix} A_x & e_5 F_x^T \\ e_3 \star^T & A_\delta \end{bmatrix} \in \mathbb{R}^{(5+3) \times (5+3)}. \quad (34)$$

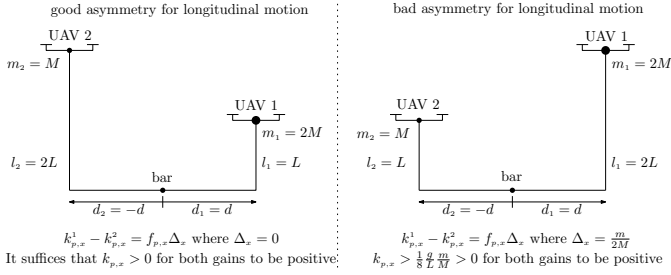


Figure 3: Good and bad asymmetries: it is better for the heavier UAV to be attached to the shorter cable as it minimizes $|\Delta_x|$. A good asymmetry only requires the gains $k_{p,x}, k_{d,x}$ to be positive, and a bad asymmetry requires both the proportional and the derivative gains to be strictly positive.

Notice that $A_{x,\delta}$ can be rendered block triangular, if one chooses the gains such that F_x in (34) vanishes. That is accomplished if the longitudinal gains are chosen as in (43), for some positive $k_{p,x}, k_{d,x}$, and k_r . That is, the proportional and derivative gains of each vehicle must be the same up to some difference that is proportional to the asymmetry of the system, as quantified by Δ_x described in (43). If the gains are chosen as in (43), then $F_x = 0_3$ and $A_{x,\delta}$ in (34) is block lower-triangular. The matrices A_x and A_δ are those in Table 1 (all parameters in Table 1 are positive, since d_1 and d_2 have opposite signs), which are both Hurwitz provided that

$$k_r > k_{p,x}/k_{d,x}, \quad (35)$$

i.e., provided that the attitude inner-loop gain is big enough. This constraint can be comprehended intuitively: fast tracking along the longitudinal direction requires a fast attitude inner-loop.

Remark 6. In (43), if one requires that $k_{p,x}^1, k_{p,x}^2 > 0$, then one must impose that $k_{p,x} > -f_p \min\left(\frac{d_1 l_1 \Delta_x, d_2 l_2 \Delta_x}{d_1 l_1 - d_2 l_2}\right)$, where Δ_x encapsulates some measure of asymmetry of the system. As illustrated in Fig. 3, there are good and bad asymmetries: in good asymmetries $\Delta_x = 0$ and, therefore, it is only required that $k_{p,x}$ be positive; and, in bad asymmetries $\Delta_x \neq 0$ and, therefore, it is required that $k_{p,x}$ be strictly positive.

Remark 7. Recall Remark 4. It follows from (34) with $F_x = 0_3$ that, for the linearized motion, (denote $X := (x^{(0)}, \dots, x^{(4)})$ and $\Delta := (\delta^{(0)}, \dots, \delta^{(2)})$)

$$\begin{bmatrix} \dot{X} \\ \dot{\Delta} \end{bmatrix} = \begin{bmatrix} A_x & 0_{5 \times 3} \\ \star_{3 \times 5} & A_\delta \end{bmatrix} \begin{bmatrix} X \\ \Delta \end{bmatrix}, \quad (36)$$

i.e., the longitudinal linear motion behaves as a fifth order integrator and it is decoupled from the longitudinal angular motion; while the longitudinal angular motion behaves as a third order integrator, cascaded after the longitudinal linear motion (A_x and A_δ are those in Table 1).

6.4.2. Lateral motion

Recall Remark 4, and note that P_y and P_ψ are associated to $A_{y,\psi} \in \mathbb{R}^{10 \times 10}$ in (33). As such, $A_{y,\psi}$ is associated with the lateral motion, namely the lateral

linear motion of the bar, and the lateral angular motion of the bar (yaw motion). In what follows denote $F_y \equiv F_y(k_{p,y}^1, k_{p,y}^2, k_{d,y}^1, k_{d,y}^2, k_{p,\psi}^1, k_{p,\psi}^2, k_{d,\psi}^1, k_{d,\psi}^2, k_r^1, k_r^2) \in \mathbb{R}^5$, where F_y is some function of the listed gains (found in the mathematica files in (Pereira and Dimarogonas, 2018)). Note then that $A_{y,\psi}$ has a specific structure, namely

$$A_{y,\psi} = \begin{bmatrix} A_y & e_5 F_y^T \\ e_5 \tilde{F}_y^T & A_\psi \end{bmatrix} \in \mathbb{R}^{(5+5) \times (5+5)}. \quad (37)$$

Notice that $A_{y,\psi}$ can be rendered block triangular, if one chooses the gains such that F_y in (37) vanishes (no choice of gains makes \tilde{F}_y vanish). That is accomplished if the lateral gains are chosen as in (44), for some positive $k_{p,y}, k_{d,y}$, and k_r . That is, the proportional and derivative gains of each vehicle must be the same up to some difference that is proportional to the asymmetry of the system, as quantified by Δ_y (and $|l_2 - l_1|$). If the gains are chosen as in (44), then $F_y = 0_5$ and $A_{y,\psi}$ in (37) is block lower-triangular. The matrices A_y and A_ψ are those in Table 1, which are both Hurwitz provided that

$$k_r > k_{p,y}/k_{d,y}, \quad (38)$$

i.e., provided that the attitude inner-loop gain is big enough. Note that similar remarks to Remarks 6 and 7 can be made at this point regarding the lateral motion.

6.4.3. Vertical motion

Recall Remark 4, and note that P_z and P_θ are associated to $A_{z,\theta} \in \mathbb{R}^{6 \times 6}$ in (33). As such, $A_{z,\theta}$ is associated with the vertical motion, namely the vertical linear motion of the bar, and the vertical angular motion of the bar (pitch motion). In what follows denote $F_z \equiv F_z(k_{p,z}^1, k_{p,z}^2, k_{d,z}^1, k_{d,z}^2, k_{i,z}^1, k_{i,z}^2) \in \mathbb{R}^3$, where F_z is some function of the listed gains. Note then that $A_{z,\theta}$ has a specific structure, namely

$$A_{z,\theta} = \begin{bmatrix} A_z & e_3 F_z^T \\ e_3 \tilde{F}_z^T & A_\theta \end{bmatrix} \in \mathbb{R}^{(3+3) \times (3+3)}. \quad (39)$$

Notice that $A_{z,\theta}$ can be rendered block triangular, if one chooses the gains such that either F_z or \tilde{F}_z in (39) vanish. We choose to cancel F_z , implying that we decouple the vertical-linear motion from the vertical-angular motion. That is accomplished if the vertical gains are chosen such that (45) is satisfied. That is, the proportional, derivative and integral gains of each vehicle must respect a ratio, which is exactly 1 under symmetry conditions (see (42)). In order to satisfy the conditions above, let, for $h \in \{p, i, d\}$ and $j \in \{1, 2\}$,

$$k_{h,z}^j = \frac{2\Delta_{z,j}}{\Delta_{z,1} + \Delta_{z,2}} k_{h,z}, \quad (40)$$

for some positive $k_{p,z}, k_{i,z}$, and $k_{d,z}$, and with $\Delta_{z,1}, \Delta_{z,2}$ as defined in (45) ($\frac{\Delta_{z,1}}{\Delta_{z,2}} > 0$ because d_1, d_2 have opposite signs). If the gains are chosen as in (40), then $F_z = 0_3$ and $A_{z,\theta}$ in (39) is block lower-triangular. The matrices A_z and A_θ are those in Table 1, which are both Hurwitz provided that (γ_z, γ_θ are positive)

$$k_{i,z} < \min(\gamma_z, \gamma_\theta) k_{p,z} k_{d,z}, \quad (41)$$

i.e., provided that the integral gain is *small enough*. Note that, for a standard PID, it is required that $k_{i,z} < k_{p,z}k_{d,z}$, while the constraint above is more restrictive, since $\gamma_\theta < 1$. Moreover, notice that γ_θ vanishes when either d_1 or d_2 vanish (the distance of the contact points to the bar's center-of-mass): as such, it is advisable to have a *large* $|d_1|$ and $|d_2|$ (*large* in the sense that $\frac{J(d_1m_1-d_2m_2)}{(-d_1d_2)m_1m_2(d_1-d_2)} \ll 1$), because γ_θ is closer to 1 (and thus the bound on the integral gain is less restrictive). This also agrees with intuition, which suggests that controlling the bar's attitude when the contact points are *too close* to the bar's center-of-mass is difficult.

We can now present our main result.

Theorem 8. *Consider the UAVs-bar system, with its vector field in (5b), the dynamic control law (16) whose internal (integral) states evolve as in (15b), and the resulting closed-loop vector field \tilde{Z}_γ^{cl} in (19). Consider also the equilibrium \tilde{z}_γ in (18), and let d_1 and d_2 have opposite signs, and the desired configuration be $\gamma = \gamma_*$ with $\theta_* = 0$ and $F_* = 0$ (i.e., the bar is to be stabilized on the horizontal plane and under no normal stress). Finally, let the longitudinal, lateral and vertical gains of the control laws be chosen as in (43), (44) and (45), respectively, and such that (i) the attitude gain is big enough, as quantified in (35) and (38); and such that (ii) the integral gain is small enough, as quantified in (41). It then follows that the equilibrium \tilde{z}_γ is exponentially stable.*

Our main result, in Theorem 8, states that pose stabilization of the bar is accomplished, provided that the UAVs-bar system starts in some neighborhood of the equilibrium. The experiments provided in (Pereira and Dimarogonas, 2017a; Pereira et al., 2018) provide insight into the region of attraction of the equilibrium; in particular, convergence to the equilibrium was verified after impulsive disturbances were applied on both the bar and the UAVs.

6.5. Bar with non-zero pitch

In this subsection, we study the effect of requiring the angular position of the bar to have a non-zero vertical component (non-zero pitch angle), i.e., when γ_* in (13) is chosen with $\theta_* \in (-\frac{\pi}{2}, \frac{\pi}{2})$ and $F_* = 0$. This equilibrium configuration corresponds to the bottom left configuration shown in Fig. 2. For this purpose, and for simplicity, we assume that the UAVs are fully-actuated, that the system is symmetric (as defined in (42)), and that no integral action is being used. Let us anticipate the results that follow, where we find out that the vertical angular motion is coupled with the longitudinal angular motion.

For this system, the Jacobian $A = d(Z_{\gamma_*}^{cl})^*(z_{\gamma_*}) \in \mathbb{R}^{24 \times 24}$ is computed, where $Z_{\gamma_*}^{cl}(z) := Z(z, u_{\gamma_*}^{pd}(z))$, with Z in (5b) ($r_i = u_i/\|u_i\|$ and \dot{r}_i ignored), z_γ in (12) and u_γ^{pd} in (16) (integral states ignored). We then compute the change of basis matrix $P \in \mathbb{R}^{24 \times 24}$, with entries listed in Table 2 (and where $P_\perp := (df(z_{\gamma_*}))^T \in \mathbb{R}^{24 \times 6}$ with f as defined in (3) – constraints invoking r_i are ignored), which renders the matrix PAP^{-1} in block triangular form (just like in (27)).

We note that $|P| = -\frac{2d^2g^6m^2\cos^2(\theta_*)}{J^2L^{10}}$ is non-zero since $\theta_* \in (-\frac{\pi}{2}, \frac{\pi}{2})$, and thus P is indeed a valid change of basis.

The diagonal entries of the matrix PAP^{-1} are listed in Table 2, and it follows that there are 5 decoupled motions, and that all matrices are Hurwitz for all $\theta_* \in (-\frac{\pi}{2}, \frac{\pi}{2})$. Indeed, it follows that the vertical linear, the longitudinal linear, the lateral linear and the lateral angular motions are all decoupled. On the other hand, it follows from $A_{\theta,s}$ that the vertical angular motion is coupled to the longitudinal angular motion when $\theta_* \neq 0$. This coupling is, nonetheless, not detrimental to the stability of the equilibrium configuration, as the matrix $A_{\theta,s}$ is Hurwitz for all $\theta_* \in (-\frac{\pi}{2}, \frac{\pi}{2})$. However, this conclusion is only valid for fully actuated UAVs; for under-actuated UAVs or for UAVs with vertical integral action, stricter conditions on the allowed interval for θ_* may be required.

6.6. Bar under non-zero normal force

In this subsection, we study the effect of requiring the bar to be under a non-zero normal force/stress, i.e., when γ_* in (13) is chosen with $\theta_* = 0$ and $F_* = r\frac{mg}{2}$, for some $r \in \mathbb{R}$. This equilibrium configuration corresponds to the top right configurations shown in Fig. 2. We note that F_* is twice the normal stress exerted on the bar and, for that reason, r represents the ratio of the normal force exerted on the bar with respect to the bar's weight. In studying this scenario, and for simplicity, we assume that the UAVs are fully-actuated, that the system is symmetric (as defined in (42)), and that no integral action is being used. Let us anticipate the results that follow, where we find out that the vertical and longitudinal motions are coupled, and that requiring the bar to be under tension is more beneficial than requiring the bar to be under compression.

For this system, the Jacobian $A = d(Z_{\gamma_*}^{cl})^*(z_{\gamma_*}) \in \mathbb{R}^{24 \times 24}$ is computed, where $Z_{\gamma_*}^{cl}(z) := Z(z, u_{\gamma_*}^{pd}(z))$, with Z in (5b) ($r_i = u_i/\|u_i\|$ and \dot{r}_i ignored), z_γ in (12) and u_γ^{pd} in (16) (integral states ignored). We then compute the change of basis matrix $P \in \mathbb{R}^{24 \times 24}$, with entries listed in Table 3 (and where $P_\perp := (df(z_{\gamma_*}))^T \in \mathbb{R}^{24 \times 6}$ with f as defined in (3) – constraints invoking r_i are ignored), which renders the matrix PAP^{-1} in block triangular form (just like in (27)).

We note that $|P| = -\frac{2d^2g^6m^2(1+r^2)^3}{J^2L^{10}}$ is non-zero for any $r \in \mathbb{R}$, and thus P is indeed a valid change of basis.

The diagonal entries of the matrix PAP^{-1} are listed in Table 3, and it follows that there are four decoupled motions. The point $p = e_1 - d\frac{J}{d^2m}re_6$ in $P_{p,\theta}$, defined in Table 3, is special in the sense that its position, velocity, acceleration and jerk (i.e., A^0p , A^1p , A^2p and A^3p) do not depend on any controller gains; this in turn guarantees that the change of basis matrix P also does not depend on any controller gains¹. It follows from the matrices listed in Table 3 that, when the bar is under normal force, the linear vertical motion is coupled with the angular longitudinal motion (where the coupling vanishes when $r = 0$);

¹In particular, when $r = 0$, then $p = e_1$ which corresponds to the longitudinal linear position of the bar.

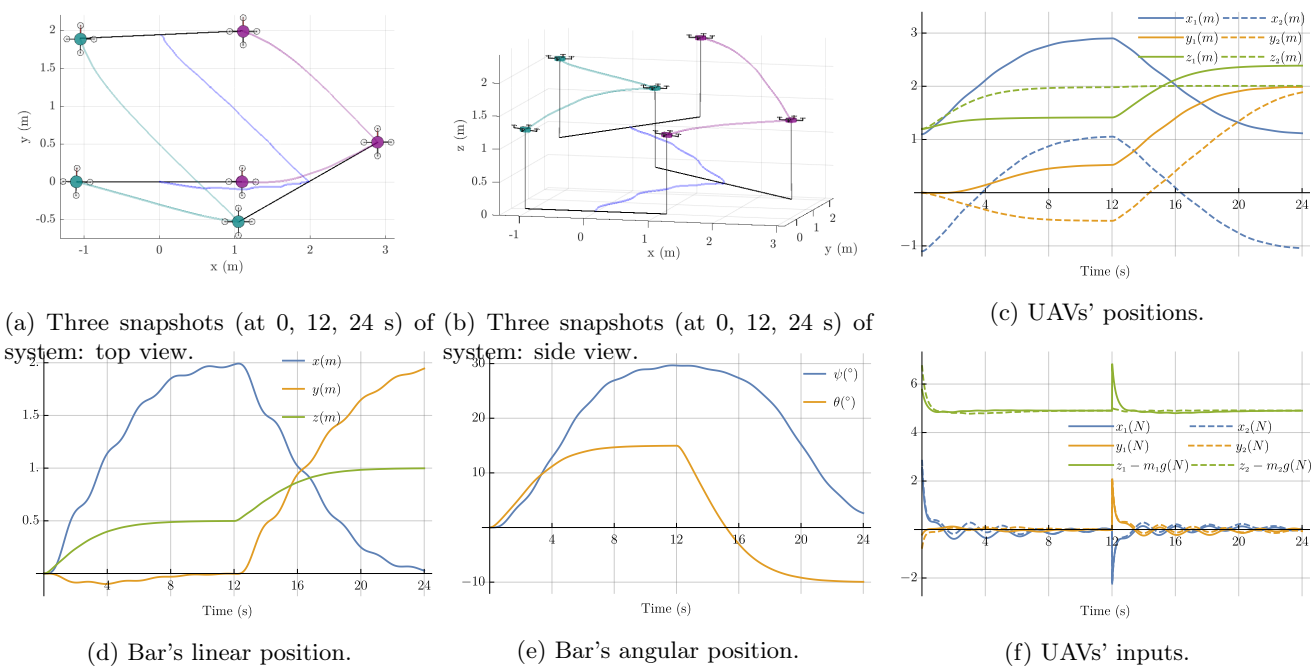


Figure 4: Simulation with two set-points with a non-zero pitch angle.

the motion of the point p (which corresponds to the linear longitudinal motion when $r = 0$) is coupled with the angular vertical motion (where the coupling vanishes when $r = 0$); where the only influence of the normal force in the linear lateral motion is to increase the frequency $f_{p,y}$ (A_y in Table 3 is Hurwitz regardless of r); and, finally, where the lateral angular motion is significantly influenced by the normal force, i.e., A_ψ in Table 3 is Hurwitz iff (note that $q_\psi(1 - \tilde{q}_\psi) = \frac{J}{d^2 m} \frac{m}{2M} \frac{1}{\delta^2} > 0$, as required by (22c))

$$k_{p,y} > -f_{p,\psi} q_\psi \tilde{q}_\psi = -\frac{g}{l} \frac{m}{2M} \frac{l}{d} r \left(1 + \frac{l}{d} \frac{r}{\sqrt{1+r^2}} \right)^{-1}.$$

This result confirms our intuition (next, and w.l.o.g., we assume that $d > 0$). For simplicity, let $d > l$. Then, when we want the bar to be under tension ($r > 0$), it suffices for the proportional gain $k_{p,y}$ to be positive; on the other hand, when we want the bar to be under compression ($r < 0$), the proportional gain $k_{p,y}$ needs to be strictly positive (and arbitrarily large, if $|r|$ is arbitrarily large). As such, one can say that requiring the bar to be under compression is less stable than requiring the bar to be under tension, because a bar under tension tends to restore the yaw position of the bar, while a bar under compression tends to destabilize the yaw position of the bar. This conclusion confirms the comments drawn during the analysis of the open-loop equilibria (see discussion after Proposition 2).

7. Experimental Results

In this Section, we provide simulations which illustrate the results discussed in Sections 6.5 and 6.6, where the bar is required to be under either a non-zero pitch angle or a non-zero normal force. Experiments illustrating the results discussed in Sections 6.3 and 6.4 are found and described

in (Pereira and Dimarogonas, 2017a; Pereira et al., 2018): the symmetric system is that illustrated in Fig. 1b, and the asymmetric is that illustrated in Fig. 1c, and videos of the experiments are found at youtu.be/ywwwPvZuVpF0 and at youtu.be/rgweowQ8fAE.

We present two simulations, in Figs. 4 and 5, illustrating, respectively, the results discussed in Sections 6.5 and 6.6. For both simulations, we consider a system with parameters $m = 1\text{kg}$; $J = 1.05\text{kgm}^2$; $m_1 = m_2 = 1.7\text{kg}$; $l_1 = l_2 = 1.2\text{m}$; $+d_1 = -d_2 = 1.1\text{m}$; and for $l \in \{x, y, z\}$, $k_{p,l} = 2.56\text{s}^{-2}$ and $k_{d,l} = 5.44\text{s}^{-1}$ (the control laws also have saturations, as discussed at the end of Section 4). For the initial condition, we let $p(0) = (0, 0, 0)m$, $n(0) = (1, 0, 0)$, $p_1(0) = (d_1, 0, l_1)m$ and $p_2(0) = (d_2, 0, l_2)m$, with vanishing linear and angular velocities. In both simulations, we let the simulation run for 24s , with one desired equilibrium $\gamma_1 \in \Gamma$ (see (9)) active from 0s to 12s , and a different desired equilibrium $\gamma_2 \in \Gamma$ active from 12s to 24s .

For both simulations, we show six figures. In Figs. 4a,5a, a top view of the system's trajectory is shown: with the bar's linear position path in blue, with the UAV's 1 position path in green, with the UAV's 2 position path in purple; and with the physical system shown at the initial time instant (initial condition described before), at the time instant when the desired equilibrium is changed, and at the final time instant. In Figs. 4b,5b, a view of the system's trajectory is shown from a different perspective. In Figs. 4c,5c, the UAVs' linear positions are shown. In Figs. 4d,5d, the bar's linear position is shown, and in Figs. 4e,5e the bar's angular position is shown parametrized by a yaw angle ψ and a pitch angle θ ($n = (\cos(\theta) \cos(\psi), \cos(\theta) \sin(\psi), -\sin(\theta))$). Finally, in Figs. 4f, 5f, the UAVs' inputs, coming from the proposed control laws, are shown.

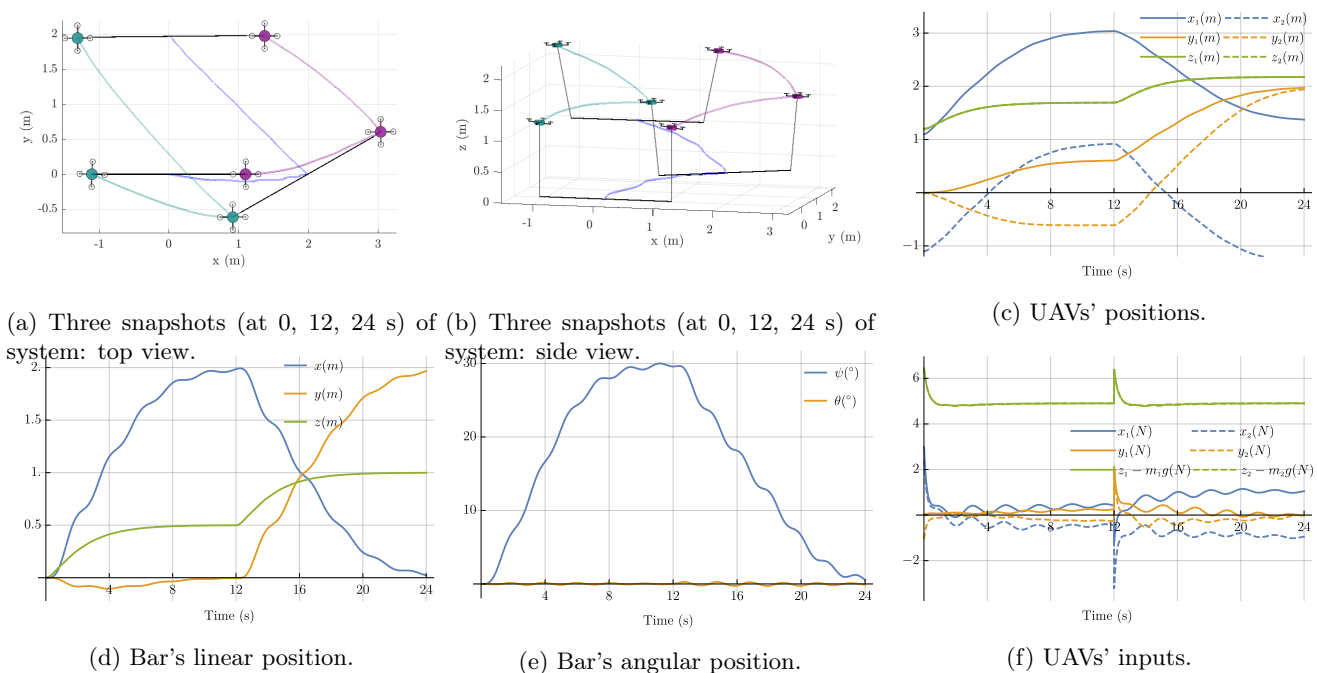


Figure 5: Simulation with two set-points with a non-zero normal force.

For the case where the bar is required to be under a non-zero pitch angle, in Fig. 4, we considered $\gamma_1 = (p, n, F)$ with $p = (2, 0, 0.5)m$, $n = (\cos(\theta) \cos(\psi), \cos(\theta) \sin(\psi), -\sin(\theta))|_{\psi=30^\circ, \theta=15^\circ}$ and $F = 0N$; and $\gamma_2 = (p, n, F)$ with $p = (0, 2, 1)m$, $n = (\cos(\theta) \cos(\psi), \cos(\theta) \sin(\psi), -\sin(\theta))|_{\psi=0^\circ, \theta=-10^\circ}$ and $F = 0N$. As discussed in Section 6.5, there is a coupling between the longitudinal-linear and the vertical-angular motions, but this coupling is not harmful to the stability. In Fig. 4b, one can visually see the positive pitch of the bar (halfway time instant) as well as the negative pitch of the bar (final time instant). Finally, in Fig. 4f, one verifies, as expected, that the vertical input force component of each UAV compensates for the UAV's weight plus half of the bar's weight; one also verifies that the horizontal input forces oscillate around zero, as the bar is not being stretched nor compressed.

For the case where the bar is required to be under a non-zero normal force, in Fig. 5, we considered $\gamma_1 = (p, n, F)$ with $p = (2, 0, 0.5)m$, $n = (\cos(\psi), \sin(\psi), 0)|_{\psi=30^\circ}$ and $F = 0.5N$; and $\gamma_2 = (p, n, F)$ with $p = (0, 2, 1)m$, $n = (\cos(\psi), \sin(\psi), 0)|_{\psi=0^\circ}$ and $F = 1N$. With these choices, it follows that the conditions $k_{p,y} > -0.24$ for γ_1 and $k_{p,y} > -0.44$ for γ_2 must be satisfied, which is indeed the case. In Fig. 5b, one can visually see that the bar is under positive normal stress, i.e., the bar is being pulled apart by the UAVs, the latter being more evident at the final time instant (when $F = 1N$) as opposed to the halfway time instant (when $F = 0.5N$). Finally, comparing Figs. 4f with 5f, one notes, as expected, that the horizontal forces are much larger when the bar is under normal stress: loosely speaking, the horizontal components of each UAV *cancel* each other (i.e., if one is *very positive*,

the other is *very negative*), since one UAV is pulling the bar in a certain direction, while the other UAV is pulling the bar in the opposite direction.

In conclusion, both simulations demonstrate that the different desired equilibria are asymptotically stable, either with a non-zero pitch angle or with a non-zero normal force. Finally, we also note that the commanded inputs, as shown in Figs. 4f, 5f, suffer a discontinuity when the desired equilibrium is changed. A smooth transition shall be considered in future work.

8. Conclusions

We proposed a control law for pose stabilization of a bar-cargo tethered to two UAVs. We modeled the system, found all its open-loop equilibria, and we closed the loop with a PID-like control law. We then provided conditions on the PID gains that guarantee that pose stabilization is accomplished. Furthermore, we described good and bad types of asymmetries, and we inferred that requiring the bar-cargo to be under tension is better for stability, as opposed to requiring the bar-cargo to be under compression. The stability properties of the equilibrium are inferred after a linearization procedure, and therefore the conclusions drawn here only hold for the original (non-linear) system on some neighborhood of the equilibrium. As such, the proposed control law is meant to be used as a back-up control law (easy to implement and tune), to be used when a more complex control law (harder to implement and tune) is being developed and tested. Future work includes experimental validation of the case where the bar is required to be pitching and under non-zero normal stress.

AEROWORKS (2018).

URL: www.aeroworks2020.eu/ (accessed 21 Nov. 2018)

- Bisgaard, M., la Cour-Harbo, A. and Bendtsen, J. D. (2010), ‘Adaptive control system for autonomous helicopter slung load operations’, *Control Engineering Practice* **18**(7), 800 – 811. Special Issue on Aerial Robotics.
- Cruz, P. J., Oishi, M. and Fierro, R. (2015), Lift of a cable-suspended load by a quadrotor: A hybrid system approach, in ‘American Control Conference’, pp. 1887–1892.
- Dai, S., Lee, T. and Bernstein, D. S. (2014), Adaptive control of a quadrotor UAV transporting a cable-suspended load with unknown mass, in ‘IEEE 53rd Annual Conference on Decision and Control’, pp. 6149–6154.
- Gassner, M., Cieslewski, T. and Scaramuzza, D. (2017), Dynamic collaboration without communication: Vision-based cable-suspended load transport with two quadrotors, in ‘IEEE International Conference on Robotics and Automation’, pp. 5196–5202.
- Goodarzi, F. A. and Lee, T. (2015), Dynamics and control of quadrotor UAVs transporting a rigid body connected via flexible cables, in ‘American Control Conference’, pp. 4677–4682.
- Jiang, Q. and Kumar, V. (2013), ‘The inverse kinematics of cooperative transport with multiple aerial robots’, *IEEE Transactions on Robotics* **29**(1), 136–145.
- Kim, S., Choi, S., Lee, H. and Kim, H. J. (2014), Vision-based collaborative lifting using quadrotor UAVs, in ‘14th International Conference on Control, Automation and Systems’, pp. 1169–1174.
- Kondak, K., Bernard, M., Caballero, F., Maza, I. and Ollero, A. (2009), ‘Cooperative autonomous helicopters for load transportation and environment perception’, *Advances in Robotics Research* pp. 299–310.
- Korpela, C., Orsag, M., Pekala, M. and Oh, P. (2013), Dynamic stability of a mobile manipulating unmanned aerial vehicle, in ‘International Conference on Robotics and Automation’, pp. 4922–4927.
- Lee, H., Kim, H. and Kim, H. J. (2017), ‘Planning and control for collision-free cooperative aerial transportation’, *IEEE Transactions on Automation Science and Engineering* **PP**(99), 1–13.
- Lee, S. J. and Kim, H. J. (2017), Autonomous swing-angle estimation for stable slung-load flight of multi-rotor UAVs, in ‘IEEE International Conference on Robotics and Automation’, pp. 4576–4581.
- Lee, T. (2014), Geometric control of multiple quadrotor UAVs transporting a cable-suspended rigid body, in ‘IEEE 53rd Annual Conference on Decision and Control’, pp. 6155–6160.
- Lee, T. (2015), Collision avoidance for quadrotor UAVs transporting a payload via voronoi tessellation, in ‘American Control Conference’, pp. 1842–1848.
- Lee, T., Sreenath, K. and Kumar, V. (2013), Geometric control of cooperating multiple quadrotor UAVs with a suspended payload, in ‘IEEE 52nd Annual Conference on Decision and Control’, pp. 5510–5515.
- Marconi, L., Naldi, R. and Gentili, L. (2011), ‘Modelling and control of a flying robot interacting with the environment’, *Automatica* **47**(12), 2571 – 2583.
- Masone, C., Bühlhoff, H. H. and Stegagno, P. (2016), Cooperative transportation of a payload using quadrotors: A reconfigurable cable-driven parallel robot, in ‘IEEE/RSJ International Conference on Intelligent Robots and Systems’, pp. 1623–1630.
- Michael, N., Fink, J. and Kumar, V. (2011), ‘Cooperative manipulation and transportation with aerial robots’, *Autonomous Robots* **30**(1), 73–86.
- Mohammadi, M., Franchi, A., Barcelli, D. and Prattichizzo, D. (2016), Cooperative aerial tele-manipulation with haptic feedback, in ‘IEEE/RSJ International Conference on Intelligent Robots and Systems’, pp. 5092–5098.
- Monforte, J. C. (2002), *Geometric Control and Numerical Aspects of Nonholonomic Systems*, Springer-Verlag.
- Nguyen, H.-N., Ha, C. and Lee, D. (2015), ‘Mechanics, control and internal dynamics of quadrotor tool operation’, *Automatica* **61**, 289 – 301.
- Nicotra, M. M., Naldi, R. and Garone, E. (2017), ‘Nonlinear control of a tethered UAV: The taut cable case’, *Automatica* **78**, 174 – 184.
- Orsag, M., Korpela, C., Pekala, M. and Oh, P. (2013), Stability control in aerial manipulation, in ‘American Control Conference’, pp. 5581–5586.
- Palunko, I., Cruz, P. and Fierro, R. (2012), ‘Agile load transportation: Safe and efficient load manipulation with aerial robots’, *IEEE Robotics Automation Magazine* **19**(3), 69–79.
- Pereira, P. O. and Dimarogonas, D. V. (2017a), Collaborative transportation of a bar by two aerial vehicles with attitude inner loop and experimental validation, in ‘IEEE 56th Annual Conference on Decision and Control’, pp. 1815–1820.
- Pereira, P. O. and Dimarogonas, D. V. (2017b), Control framework for slung load transportation with two aerial vehicles, in ‘IEEE 56th Annual Conference on Decision and Control’, pp. 4254–4259.
- Pereira, P. O. and Dimarogonas, D. V. (2017c), Nonlinear pose tracking controller for bar tethered to two aerial vehicles with bounded linear and angular accelerations, in ‘IEEE 56th Annual Conference on Decision and Control’, pp. 4260–4265.
- Pereira, P. O. and Dimarogonas, D. V. (2017d), Stability of load lifting by a quadrotor under attitude control delay, in ‘IEEE International Conference on Robotics and Automation’, pp. 3287–3292.
- Pereira, P. O. and Dimarogonas, D. V. (2018), Mathematica files used in obtaining the manuscript’s results with a companion extended paper version, in ‘<https://github.com/KTH-SML/pose-stabilization-of-bar-tethered-to-two-uavs.git>’.
- Pereira, P. O., Roque, P. and Dimarogonas, D. V. (2018), Asymmetric collaborative bar stabilization tethered to two heterogeneous aerial vehicles, in ‘2018 IEEE International Conference on Robotics and Automation’, pp. 5247–5253.
- Pounds, P. E. I. and Dollar, A. M. (2014), ‘Stability of helicopters in compliant contact under PD-PID control’, *IEEE Transactions on Robotics* **30**(6), 1472–1486.
- Schmidt, G. and Swik, R. (1974), ‘Automatic hover control of an unmanned tethered rotorplatform’, *Automatica* **10**(4), 393 – 403.
- Suarez, A., Heredia, G. and Ollero, A. (2016), Lightweight compliant arm with compliant finger for aerial manipulation and inspection, in ‘IEEE/RSJ International Conference on Intelligent Robots and Systems’, pp. 4449–4454.
- Tagliabue, A., Kamel, M., Verling, S., Siegwart, R. and Nieto, J. (2017), Collaborative transportation using MAVs via passive force control, in ‘IEEE International Conference on Robotics and Automation’, pp. 5766–5773.
- Tang, S. and Kumar, V. (2015), Mixed integer quadratic program trajectory generation for a quadrotor with a cable-suspended payload, in ‘IEEE International Conference on Robotics and Automation’, pp. 2216–2222.
- Tognon, M., Dash, S. S. and Franchi, A. (2016), ‘Observer-based control of position and tension for an aerial robot tethered to a moving platform’, *IEEE Robotics and Automation Letters* **1**(2), 732–737.
- Tognon, M. and Franchi, A. (2017), ‘Dynamics, control, and estimation for aerial robots tethered by cables or bars’, *IEEE Transactions on Robotics* **33**(4), 834–845.

Change of basis	Decoupled state matrices	Parameters when (42) holds	Parameters
$P_x := [e_1 \ Ae_1 \ A^2e_1 \ A^3e_1 \ A^4e_1]$	$A_x = \Gamma_5(q_x, (f_{p,x}, k_r), (k_{p,x}, k_{d,x}))$	$f_{p,x} = \frac{q}{l}, q_x = \frac{m}{2M}$	$f_{p,x} = \frac{g(d_1l_1 - d_2l_2)}{l_1l_2(d_1 - d_2)}, q_x = \frac{m(d_1^2l_1^2m_1 + d_2^2l_2^2m_2)}{m_1m_2(d_1l_1 - d_2l_2)^2}$
$P_\delta := [\nu \ A\nu \ A^2\nu] _{\nu=e_7-e_{10}}$	$A_\delta = \Gamma_3(\tilde{f}_{p,x}, (k_{p,x}, k_{d,x}))$	$\tilde{f}_{p,x} = \frac{q}{l} \frac{m}{2M}$	$\tilde{f}_{p,x} = \frac{gm(d_1^2l_1^2m_1 + d_2^2l_2^2m_2)}{l_1l_2m_1m_2(d_1 - d_2)(d_1l_1 - d_2l_2)}$
$P_y := [e_2 \ Ae_2 \ A^2e_2 \ A^3e_2 \ A^4e_2]$	$A_y = \Gamma_5(q_y, (f_{p,y}, k_r), (k_{p,y}, k_{d,y}))$	$f_{p,y} = \frac{q}{l}, q_y = \frac{m}{2M}$	$f_{p,y} = \frac{g(d_1l_1 - d_2l_2)}{l_1l_2(d_1 - d_2)}, q_y = \frac{m(d_1^2l_1^2m_1 + d_2^2l_2^2m_2)}{m_1m_2(d_1l_1 - d_2l_2)^2} + \frac{-md_1d_2 - d_1d_2(l_1 - l_2)^2}{j(d_1l_1 - d_2l_2)^2}$
$P_\psi := [e_5 \ Ae_5 \ A^2e_5 \ A^3e_5 \ A^4e_5]$	$A_\psi = \Gamma_5(q_\psi, (f_{p,\psi}, k_r), (k_{p,\psi}, k_{d,\psi}))$	$f_{p,\psi} = \frac{d^2m}{j} f_{p,y}, q_\psi = \frac{j}{d^2m} q_y$	$f_{p,\psi} = \frac{-md_1d_2}{j} f_{p,y}, q_\psi = \frac{j}{-md_1d_2} q_y$
$P_z := [\nu \ A\nu \ A^2\nu] _{\nu=\frac{d_2e_{31}-d_1e_{32}}{d_2-d_1}}$	$A_z = C_3(\gamma_z(k_{i,z}, k_{p,z}, k_{d,z}))$	$\gamma_z = \left(1 + \frac{m}{2M}\right)^{-1}$	$\gamma_z = \gamma_\theta \frac{\Delta_{z,1}\Delta_{z,2}}{(d_1d_2(d_1 - d_2)m_1m_2)^2} \frac{1}{1 + \frac{m(d_1^2m_1 + d_2^2m_2 + j(m_1 + m_2))}{(d_1 - d_2)^2 m_1 m_2}}$ see (45)
$P_\theta := [\nu \ A\nu \ A^2\nu] _{\nu=\frac{e_{31}-e_{32}}{d_2-d_1}}$	$A_\theta = C_3(\gamma_\theta(k_{i,z}, k_{p,z}, k_{d,z}))$	$\gamma_\theta = \left(1 + \frac{j}{d^2m} \frac{m}{2M}\right)^{-1}$	$\gamma_\theta = \left(1 + \frac{j(d_1m_1 - d_2m_2)}{2(-d_1d_2)m_1m_2(d_1 - d_2)}\right)^{-1}$

Table 1: Decoupled state matrices with $\theta_* = 0$ and $F_* = 0$ (no pitch and no normal force). Matrices Γ_5, C_3 defined in Section 5.

Change of basis	Decoupled state matrices	Parameters
$P_z := [e_3 \ Ae_3]$	$A_z = C_2(\gamma_z(k_{p,z}, k_{d,z}))$	$\gamma_z = \left(1 + \frac{m}{2M}\right)^{-1}$
$P_{\theta,\delta} := [e_6 \ Ae_6 \ \nu \ A\nu] _{\nu=e_7-e_{10}}$	$A_{\theta,\delta} = \begin{bmatrix} C_2(-\gamma_\theta(k_{p,z} + \tan(\theta_*)f_{p,x}, k_{d,z})) & -\frac{f_{p,x}}{2d}\gamma_\theta \tan(\theta_*)e_2e_1^T \\ -2d \tan(\theta_*)f_{p,x}e_2e_1^T & C_2(-(k_{p,x} + f_{p,x}, k_{d,x})) \end{bmatrix}$	$\gamma_\theta = \left(1 + \frac{j}{d^2m} \frac{m}{2M} \cos(\theta_*)\right)^{-1}, f_{p,x} = \frac{q}{l} \frac{m}{2M}$
$P_x := [e_1 \ Ae_1 \ A^2e_1 \ A^3e_1]$	$A_x = \Gamma_4(q_x, f = (f_{p,x}, k_r), (k_{p,x}, k_{d,x}))$	$f_{p,x} = \frac{q}{l}, q_x = \frac{m}{2M}$
$P_y := [e_2 \ Ae_2 \ A^2e_2 \ A^3e_2]$	$A_y = \Gamma_4(q_y, f_{p,y}, k = (k_{p,y}, k_{d,y}))$	$f_{p,y} = \frac{q}{l}, q_y = \frac{m}{2M}$
$P_\psi := [e_5 \ Ae_5 \ A^2e_5 \ A^3e_5]$	$A_\psi = \Gamma_4(q_\psi, f_{p,\psi}, k = (k_{p,\psi}, k_{d,\psi}))$	$f_{p,\psi} = \frac{d^2m}{j} f_{p,y}, q_\psi = \frac{j}{d^2m} q_y$

Table 2: Decoupled state matrices when bar is required to have non-zero pitch angle θ_* . Matrices Γ_4, C_2 defined in Section 5.

$$l_1 = l_2 =: l > 0, d_1 = -d_2 =: d \in \mathbb{R} \setminus \{0\}, m_1 = m_2 =: M > 0, k_{i,h}^1 = k_{i,h}^2 =: k_{i,h}^1 = k_{i,h}^2 =: k_r^1 = k_r^2 =: k_r^j > 0, k_{p,\psi}^j = 0, k_{d,\psi}^j = 0. \quad (42)$$

$$F_x = 0_3 \Leftrightarrow k_{p,x}^j = k_{p,x} + \frac{d_j l_j}{d_1 l_1 - d_2 l_2} f_{p,x} \Delta_x, k_{d,x}^j = k_{d,x} + \frac{d_j l_j}{d_1 l_1 - d_2 l_2} f_{p,x} \Delta_x, k_r^1 = k_r^2 = k_r^j = k_r, \Delta_x = \frac{m(d_1 l_1 m_1 + d_2 l_2 m_2)}{m_1 m_2 (d_1 l_1 - d_2 l_2)}, \quad (43)$$

$$F_y = 0_5 \Leftrightarrow \begin{cases} k_{p,y}^j = k_{p,y} + \frac{d_j l_j}{d_1 l_1 - d_2 l_2} f_{p,y} \Delta_y \\ k_{d,y}^j = k_{d,y} + \frac{d_j l_j}{d_1 l_1 - d_2 l_2} f_{p,y} \Delta_y \end{cases}, \begin{cases} k_r^j = k_r^2 = k_r \\ \Delta_y = \frac{m(d_1 l_1 m_1 + d_2 l_2 m_2)}{m_1 m_2 (d_1 l_1 - d_2 l_2)} + \frac{-md_1 d_2 (d_1 - d_2)(l_1 - l_2)}{j(d_1 l_1 - d_2 l_2)^2} \end{cases}, \quad (44)$$

$$F_z = 0_3 \Leftrightarrow \begin{cases} k_{i,z}^1 = k_{i,z}^2 = k_{i,z}^j = k_{i,z}^j = k_{i,z}^j = k_{i,z}^j = k_{i,z}^j \\ k_{p,z}^1 = k_{p,z}^2 = k_{p,z}^j = k_{p,z}^j = k_{p,z}^j = k_{p,z}^j = k_{p,z}^j \\ k_{d,z}^1 = k_{d,z}^2 = k_{d,z}^j = k_{d,z}^j = k_{d,z}^j = k_{d,z}^j = k_{d,z}^j \end{cases} =: \Delta_{z,1} \quad \Delta_{z,2}. \quad (45)$$

Change of basis	Decoupled state matrices	Parameters
$P_{z,\delta} := [e_3 \ Ae_3 \ \nu \ A\nu] _{\nu=e_7-e_{10}}$	$A_{z,\delta} = C_2(-\gamma_z(k_{p,z}, k_{d,z})) \oplus C_2(-(k_{p,x} + f_{p,x}, k_{d,x})) + \mathcal{O}(r)$	$\gamma_z = \left(1 + \frac{m}{2M}\right)^{-1}, f_{p,x} = \frac{q}{l} \frac{m}{2M}$
$P_{p,\theta} := [e_6 \ Ae_6 \ p \ Ap \ A^2p \ A^3p]$	$A_{p,\theta} = C_2(-\gamma_\theta(k_{p,x}, k_{d,x})) \oplus \Gamma_4(q_x, f_{p,x}, (k_{p,x}, k_{d,x})) + \mathcal{O}(r)$	$\gamma_\theta = \left(1 + \frac{j}{d^2m} \frac{m}{2M}\right)^{-1}, f_{p,x} = \frac{q}{l}, q_x = \frac{m}{2M}$
$P_y := [e_2 \ Ae_2 \ A^2e_2 \ A^3e_2]$	$A_y = \Gamma_4(q_y, f_{p,y}, (k_{p,y}, k_{d,y}))$	$f_{p,y} = \frac{q}{l} \sqrt{1 + r^2}, q_y = \frac{m}{2M}$
$P_\psi := [e_5 \ Ae_5 \ A^2e_5 \ A^3e_5]$	$A_\psi = \tilde{\Gamma}_4(\tilde{q}_\psi, q_\psi, f_{p,\psi}, (k_{p,\psi}, k_{d,\psi}))$	$f_{p,\psi} = \frac{d^2m}{j} \delta f_{p,y}, q_\psi = \frac{j}{d^2m} \delta^{-1} q_y, \tilde{q}_\psi = \frac{\delta - 1}{\delta}, \delta = \left(1 + \frac{l}{d} \frac{r}{\sqrt{1+r^2}}\right)$

Table 3: Decoupled state matrices when bar is required to be under a non-zero normal force F_* (where $p = e_1 - d \frac{j}{d^2m} r e_6$). Matrices $\Gamma_4, \tilde{\Gamma}_4, C_2$ defined in Section 5.